Coversheet for EarthArXiv

Volcanic CO_2 degassing and microbial carbon fixation in a caldera offshore

Sandoval-Velasquez A.[1,2], Migliaccio, F.[2,3], Diana, S. C.[1,2], Caliro, S.[4], de Ruggiero P.[5], Di Vito, M.A.[4], Milazzo M.[1,2], Sgubin, G.[1], Giovannelli, D.[2,3,6,7,8,9], Aiuppa, A.[1,2]

[1] DiSTeM, Università di Palermo, Palermo, Italy
[2]National Biodiversity Future Center, Palermo, Italy
[3]Department of Biology, University of Naples Federico II, Napoli, Italy
[4]Osservatorio Vesuviano, Istituto Nazionale di Geofisica e Vulcanologia, Napoli, Italy
[5]Dipartimento di Scienze e Tecnologie (DIST), Università degli Studi di Napoli "Parthenope", Napoli, Italy
[6]Institute of Marine Biological Resources and Biotechnologies, National Research Council, Ancona, Italy
[7]Earth-Life Science Institute, Tokyo Institute for Technology, Tokyo, Japan
[8]Marine Chemistry and Geochemistry Department, Woods Hole Oceanographic Institution, Woods Hole, MA, USA
[9]Department of Marine and Coastal Science, Rutgers University, New Brunswick, NJ, USA

Volcanic CO_2 degassing and microbial carbon fixation in a caldera offshore

Sandoval-Velasquez A.[1,2], Migliaccio, F. [2,3], Diana, S. C. [1,2], Caliro, S.[4], de Ruggiero P.[5], Di Vito, M.A.[4], Milazzo M.[1,2], Sgubin, G.[1], Giovannelli, D. [2,3,6,7,8,9], Aiuppa, A. [1,2]

[1] DiSTeM, Università di Palermo, Palermo, Italy
[2]National Biodiversity Future Center, Palermo, Italy
[3]Department of Biology, University of Naples Federico II, Napoli, Italy
[4]Osservatorio Vesuviano, Istituto Nazionale di Geofisica e Vulcanologia, Napoli, Italy
[5]Dipartimento di Scienze e Tecnologie (DIST), Università degli Studi di Napoli "Parthenope", Napoli, Italy
[6]Institute of Marine Biological Resources and Biotechnologies, National Research Council, Ancona, Italy
[7]Earth-Life Science Institute, Tokyo Institute for Technology, Tokyo, Japan
[8]Marine Chemistry and Geochemistry Department, Woods Hole Oceanographic Institution, Woods Hole, MA, USA
[9]Department of Marine and Coastal Science, Rutgers University, New Brunswick, NJ, USA

Calderas are subsided volcanic terrains formed by the destructive power of some of the largest volcanic eruptions on Earth. Many such depressions globally are today submerged by crater lakes or seawater, rendering them less accessible to scientific scrutiny, and hence more complicated to monitor during unrest. One of such systems is the restless, partly submerged Campi Flegrei caldera (CFc) near Naples in Italy, where escalating hydrothermal activity during ongoing unrest demands for an improved understanding of the caldera offshore. Here, we present a high-resolution, system-wide mapping of CO_2 degassing encompassing the caldera offshore and onshore sectors. Combining vertical seawater profiles with groundwater composition results, we obtain a refined delimitation of the anomalous CO_2 degassing zones, finding an overall structural control on volatile transport and surface/seafloor discharge. Intense CO_2 degassing on the seafloor also causes ocean acidification, sustains diverse chemolithotrophic communities near the hydrothermal emissions, and influences the near-vent environment, as demonstrated by taxonomic and functional diversity data. Submerged caldera sectors are extremely dynamic environments whose volcanological significance and biogeochemistry may have been overlooked.

Calderas are volcanic depressions formed by volcano subsidence in response to rapid drainage of magma during large-scale volcanic eruptions[1]. Owing to their depressed morphologies, subaerial calderas are recurrently filled with meteoric water forming crater lakes[2], or invaded by seawater in the offshore of coastal volcanoes. Because submerged calderas escape direct observation from surface, their monitoring poses significant technical challenges to volcanologists, and render these geological objects systematically less well understood than their subaerial equivalents. For example, hydrothermal fluid venting potentially occurs at many, if not all, submarine caldera floors, but information on chemistry and flux of such manifestations remains limited to a relatively small number of better studied systems[3]. In a few cases, the fluid geochemistry of flooded or partially flooded caldera depressions has been

investigated from surveys on the effects of CO_2-rich seepages on shallow marine areas, with notable examples from the Maug Caldera (Northern Mariana Islands)[4], the harbour of Matupi within the Rabaul caldera (Papua New Guinea)[5], Levante Bay on the island of Vulcano (Italy) and Mikama Bay in Shikine Island (Japan)[6,7]. Nevertheless, the extent to which these submersed or semi-submersed caldera systems contribute to the overall (volcano-scale) budget of magma-sourced volatiles remains undetermined.

Degassing of CO_2 and reduced volatiles in submarine calderas also supports exceptionally diverse microbial communities, sustained by both photosynthesis and chemosynthesis depending on depth and light penetration[8]. Microbial communities present in the subsurface directly use CO_2 and reduced volatiles (H_2, H_2S, CO, CH_4, Fe^{2+}, etc..) of hydrothermal and magmatic origin to sustain chemolithoautotrophy[8,9]. Similarly high biomass can be found in the venting fluids and in complex biofilm forming at venting sites on the seafloor [8,10–12]. The organic carbon produced by the microbial communities using volcanic reduced compounds can be exported, together with nutrients, trace metals and reduced compounds, to neighbouring ecosystems [13,14] and higher trophic levels in the area, thus potentially supporting hot spots of biological activity[15]. In addition to this, subsurface microbial communities interacting with volatiles of volcanic and mantle origin have been shown to be able to alter their composition and the quantity of volatiles reaching the atmosphere, potentially impacting volatile budgets in volcanic regions[16–18]. In spite of this, the microbial diversity associated with hydrothermal activity in submerged calderas and its biogeochemical contributions to volatile cycling has received limited attention, and the extent of the influence of volatile degassing from submarine calderas to surrounding marine ecosystems remains largely unknown[15].

The Campi Flegrei caldera (CFc), on the Neapolitan coast of southern Italy (Fig. 1a), is one of the most densely inhabited and hence hazardous in the world. The caldera has been increasingly monitored in response to a ground deformation, seismic and degassing unrest that, started in 1950-52[19], has continued with alternating vigor until present[20], with a remarkable intensification since 2018[21]. Gradual caldera inflation during 4 main unrest episodes (1950–52, 1970–72, 1982–84, and 2005-present) has caused a total net uplift[22] of > 4m in the area of maxim uplift (Pozzuoli town), at the centre of the resurgent caldera block[23]. Uplift has also been accompanied by intense shallow (< 4 km) volcano-tectonic seismicity[24–27], especially during two intense uplift phases (known as bradyseismic crises) of 1982-84 and 2005-present, and by a visible escalation in hydrothermal degassing activity[28].

Hydrothermal manifestations within the northern, emerged half of the caldera (Fig. 1) have intensively been studied and monitored, and their temporally changing compositions and fluxes have provided evidence for a sizeable escalation in magma-sourced CO_2 release from the fumaroles[29,30] and diffusively through degassing soils[31] and aquifers[32]. However, the extent to which this CO_2 escalation also extends to the caldera offshore remains comparatively less known[33]. This southern, submerged CF caldera sector (Fig. 1) has increasingly been studied using geophysical prospection tool, allowing for a refined

understanding of caldera floor morphology[34], and of its geological[35] and structural[35–39] setting and evolution, including the effects of relative sea water changes and their interplay with human settling and infrastructures dating back the roman time[40,41]. Marine geology prospecting has also provided observational evidence for an intense degassing of magmatic fluids on the submerged caldera floor[34], but direct measurements on the chemistry of such submarine hydrothermal vents have been limited to a few cases[33], and the impact of vent emissions on the chemistry and biology of the overlying seawater column and on the surrounding ecosystems is poorly understood. Studies on the microbiology and ecosystems impact of the CFc degassing are limited to a preliminary description of the microbial diversity associated with the fluids and biofilms of some shallow-water hydrothermal vents in the shallower parts of the caldera[12] and an investigation of the sedimentary meiofauna diversity associated with a single vent[42].

Results

Offshore pCO_2

We conducted a systematic survey across the Pozzuoli Bay (Fig. 1b), during which we characterized degassing activity in the CFc offshore by measuring the CO_2 partial pressure (pCO_2) in the seawater column at 273 vertical profiles (see Methods and Supplementary Table 1). Our large dataset (520 punctual measurements) constrain the mean and median pCO_2 values at 574 and 505 µatm, respectively (± 1 standard deviation of 502 µatm). This is well above the typical atmospheric equilibrium pCO_2 value of 420 µm[43], indicating the existence of an additional CO_2 source in excess to atmospheric CO_2.

We identify a large spatial heterogeneity in pCO_2 values across the bay (Fig. 2), suggesting that such excess CO_2 is not uniformly distributed, but rather focused in specific areas. Approximately 80% of seawater measurements fall within a relatively narrow range, from approximately 376 µatm to 600 µatm (Figs. 2a to 5). However, significantly higher concentrations are observed at a number of sites, revealing a "hotspot" distribution. These localized, high-concentration zones cluster in 5 main areas where CO_2-rich hydrothermal vents have been reported in the seafloor (Fig. 2a, 3):

Secca delle Fumose (SdF): This area is known since antiquity for the presence of hydrothermal CO_2 vents[33,44] distributed along pillars of Roman age of unknown use (Supplementary Figures 1a, b). This site exhibits the most extreme pCO_2 conditions observed, and was therefore selected for coupling pCO_2 measurements with microbial diversity analysis in a series of water column transects (Fig. 2b). A vertical profile was conducted in the SdF area, right above the SdF vents, each consisting of pCO_2 measurements at 2, 6, and 10 m depth (Fig. 3a and Supplementary Table 2). This profile demonstrates a steep CO_2 vertical gradient along the water column which leads to a rapid decline in seawater pH. At 2 m, pCO_2 ranges from 500–520 µatm (pH = 8.02), suggesting only moderate enrichment relative to ambient seawater. At 6 m, pCO_2 increases substantially, reaching 1400–1600 µatm (pH = 6.94). The

highest values are recorded at 9-10 m, where pCO_2 peaks at 6800 to 9000 µatm (pH = 5.77). In conjunction with nearby profiles, these observations identify a clear CO_2 plume originating from the seafloor, and propagating upward along the seawater column (Fig. 3a, 3b). Orange and green colored biofilm are present in the area of focused venting (Supplementary Figure 2) while white biofilms are present in the area of lower temperature diffuse degassing (Supplementary Figures 3 and 4).

Baia Castle beach: Here, pCO_2 levels are elevated but remain substantially lower than those recorded at SdF (Figs. 2-3b). Owing to the shallow seafloor, only a single depth measurement was possible. pCO_2 measured at 3 m reached a maximum of 849 µatm. Although this value indicates moderate CO_2 enrichment, free gas bubbles were observed rising from the substrate at this location, confirming the presence of localized venting activity. The limited water depth prevented assessment of a vertical gradient, yet the measurement and visual observations together characterize Baia as a site influenced by mild but detectable CO_2 seepage.

Capo Miseno: Bubbling activity has systematically been reported in the Capo Miseno area, both at the seafloor and at the air-seawater interface, and was clearly visible during our campaign (Supplementary Figures S1c, d). Here, our results identify two spatially distinct CO_2-emitting hotspots. The first occurs within the Gulf of Miseno, between Isola Pennata and Punta Sarparella (Fig. 3c). In this area, 22 vertical profiles were conducted, with measurements at 1–2 m and 7–10 m depth (water depth reached ~20 m at stations near the gulf entrance). pCO_2 values increase with depth and are uniformly elevated ranging from 540 to 1700 µatm across profiles. A second CO_2-rich spot is identified south of Capo Miseno, in the vicinity of the Faro (Fig. 3c and Supplementary Figure 5). Free gas emissions in this site were visibly more intense than in the gulf, with continuous bubble release reaching the surface, indicating stronger localized venting. Here, a detailed profile was completed with measurements at two depths: pCO_2 at 1–2 m is ~590 µatm, while at 7–8 m it increases substantially, ranging from 610 to 2300 µatm. Although more localized than the first hotspot, this site similarly exhibits a pronounced increase in pCO_2 with depth.

Academia-Bagnoli area: A total of 62 vertical profiles are conducted along the Accademia and Bagnoli coastlines, representing the most spatially extensive survey area in this study. Profiles closest to the shoreline—where the highest pCO_2 values are recorded—consist of a single measurement at 1–2 m depth due to the shallow seafloor. In contrast, offshore profiles include two or three depth layers (1–2 m, 3–7 m, and 9–15 m), depending on local bathymetry. The highest pCO_2 values in this area are measured along the Bagnoli coastline, particularly in proximity to the Pontile Nord. Here, pCO_2 reached a maximum of 4420 µatm, with additional peaks of 882 and 2450 µatm recorded at nearby points. Free gas bubbles are frequently observed rising from the seabed, confirming the presence of active degassing. In the Accademia sector, pCO_2 levels are lower (576–732 µatm) but still markedly elevated relative to typical atmospheric equilibrium concentrations (Fig. 2, 3b).

Nisida: The Nisida island offshore is a significant CO_2-emitting spot within the Gulf of Pozzuoli (Figs. 2-3b). Elevated pCO_2 levels are detected at the base of the peninsula, particularly in the area facing the Lega Navale di Pozzuoli and the Dente di Cane rocky outcrop. A total of 35 vertical profiles are conducted across the area, allowing characterization of both nearshore and offshore variability. At 1–2 m depth, pCO_2 ranges from 800 to 1100 µatm, indicating a localized but persistent CO_2 excess reactive to air-saturated seawater.

Measurements of seawater pCO_2 were not possible in three sectors of the Pozzuoli Bay due to access limitations and maritime regulations (Figure 1b). These include (i) the interior of the Pozzuoli harbour, where active venting has been reported but could not be surveyed because of restrictions on boat operations; (ii) the high-traffic navigation corridor used by local ferries, which is excluded from scientific access for safety reasons; and (iii) an area of approximately 0.723 m² southwest the SdF occupied by a mytilid aquaculture facility, where safe operation of powerboats is not feasible. Although these sectors were interpolated in the spatial analysis, they may host additional CO_2 sources, implying that our estimates of offshore degassing are likely conservative.

Onshore pCO_2

CO_2 degassing in the onshore CFc sector is evidenced by high pCO_2 values (n = 83) measured in groundwater samples. In this study, pCO_2 was recalculated in µatm using data previously reported in the literature[32] (Methods, and Fig. 1b, 4). The extremely high values encountered reflect the large, widespread interaction of the groundwater system with deep-rising magmatic CO_2, sourced by the underlying magma plumbing system[45]. Groundwater pCO_2 displays a broad range, from 317 µatm to 867961 µatm. The mean pCO_2 is 116512±208011 µatm (mean ± standard deviation), with a median of 21429 µatm. 67% of all land-based measurements exceed 10000 µatm, and 29% exceed 50,000 µatm. CO_2 enrichment is the largest in a wide degassing area centered on Solfatara crater, the largest degassing structure in the caldera onshore[28], and stretching from Pozzuoli town to the west to Agnano-Bagnoli to the east (Fig. 4). A second, less prominent CO_2 degassing zone is identified on the west, in the Baia-Averno-Monte Nuovo area (Fig. 4).

Microbial diversity in the hydrothermal vent environment

Geochemical pCO_2 surveys were coupled with fluid, biofilm, and seawater sampling to investigate the effects of hydrothermal venting on microbial diversity. Between June and July 2023, divers collected hydrothermal fluids (73 °C) and biofilm samples directly from the SdF vent at 10 m depth, as well as biofilms associated with lower-temperature (30–40 °C) diffuse venting within the same hydrothermal area. In October 2024, seawater column samples were collected along N–S and E–W transects centered on the SdF vent (n = 9 water column stations, for a total of 21 samples at different depths; Fig. 2b). These samples are part of a broader framework of biological sampling efforts aimed at characterizing microbial diversity in the Gulf of Pozzuoli.

Shotgun metagenomic sequencing generated 6,997 million reads across all samples (a mean of 259 million reads per sample), of which 99% passed quality filtering. Of these, 802 million paired reads (23%) were taxonomically annotated. The vent fluid sample (SF1D13_F2) was dominated by Aquificota (53.99% of annotated sequences), largely represented by the Hydrogenothermaceae family (50.75%; Fig. 6). Biofilm samples were dominated by a limited number of phyla but showed marked compositional differences. The biofilm collected at the SdF vent orifice (SF1D13_B1) was strongly dominated by Cyanobacteriota (36.55%), whereas a second biofilm from the same vent (SF1D13_B2) was enriched in Aquificota (22.89%), with Hydrogenothermaceae accounting for 21.46% of the community. Microbial white mats collected from lower-temperature diffuse emission sites (SF2A_B1, SF2B_B1, SF2C_B1) shared the same dominant phyla but exhibited a clear compositional shift across samples. Pseudomonadota decreased from 32.23% (SF2A_B1) to 12.08% (SF2C_B1), while Campylobacterota increased from 2.91% to 15.45% of total reads. Within Campylobacterota, Sulfurovaceae ranked among the most abundant families in SF2B_B1 (2.69%) and SF2C_B1 (1.99%), whereas Thiovulaceae peaked in SF2C_B1 (6.33%). These all represent known groups of thermophilic and mesophilic chemolithoautotrophic microorganisms capable of hydrogen, sulfide and thiosulfate oxidation at the expenses of nitrate or oxygen[46–48].

Seawater samples displayed a broadly homogeneous background community at the phylum level, dominated by Pseudomonadota (mean ~47.45%, range 29.65–72.85%) and Bacteroidota (mean ~13.53%, range 3.36–22.66%; Fig. 6), while Cyanobacteriota and Verrucomicrobiota remained minor components. At the family level, Alteromonadaceae, Pelagibacteraceae, Flavobacteriaceae, Paracoccaceae, and Halieaceae were consistently among the most abundant. Some samples showed localized enrichments in less ubiquitous families (*e.g.*, Halomonadaceae, Vibrionaceae), including clear outliers such as T7D1, where Pseudoalteromonadaceae reached 14.49%. These sequences represent well known coastal water column microbial groups involved in oxygenic photosynthesis (sequences belonging to the Cyanobacterota) or in organic matter cycling[49,50].

Compositional differences among samples were assessed using beta diversity analysis based on weighted Jaccard dissimilarity (Fig. 7a). Seawater samples clearly separated from biofilms and hydrothermal fluids along the main PCoA axis, which captured 36.5% of the total variance. Within seawater samples, separation reflected the degree of hydrothermal influence, primarily associated with pH variations along the first and second ordination axes, with PCoA1 correlating with pH (Fig. 7b, Pearson correlation, $r^2 = 0.549$, $p = 0.012$). This separation was driven by microbial groups typically associated with hydrothermal emissions, which were abundant in vent fluids and biofilms (Fig. 8). These families constituted up to 50% of annotated sequences in hydrothermal-associated samples (Fig. 8a), but remained rare in seawater (<0.1% on average), showing systematic increases with decreasing distance from the vent and increasing depth, consistent with dilution during plume mixing (Fig. 8b).

The distribution of genes encoding key biogeochemical functions mirrored the taxonomic patterns (Fig. 9). PCoA of functional gene composition based on weighted Jaccard dissimilarity showed a clear separation between seawater and hydrothermal-associated samples along the main axis, accounting for 51.3% of the variance (Fig. 9a) when using all the biogeochemical genes, while the second axis explained only 9.3%. Genes of the Calvin–Benson–Bassham (CBB) cycle and the 3-hydroxypropionate (3HB) bicycle were widespread across all samples (Fig. 9b). In contrast, genes encoding the reductive tricarboxylic acid (rTCA) cycle and the Wood–Ljungdahl (WL) pathway were enriched in vent fluids and biofilms, reflecting their association with facultative microaerophilic and anaerobic microorganisms typical of hydrothermal systems. Nevertheless, these genes were also detected in seawater samples, consistent with plume-mediated transport of vent-associated microorganisms and metabolic potential (Fig. 9b).

Vent fluids and biofilm samples shared a pronounced sulfur cycling potential, being enriched in genes involved in thiosulfate disproportionation, sulfur, sulfite, and sulfate oxidation, as well as sulfate reduction (Fig. 9c). Sulfur cycling genes were also detected in seawater, albeit at lower abundances, particularly those involved in thiosulfate disproportionation and sulfide oxidation. While present across all sample types, genes associated with thiosulfate oxidation were relatively enriched in seawater compared to SdF biofilms, suggesting that this metabolism is favored under the more oxidizing conditions characteristic of plume mixing zones.

Discussion

Caldera offshores as potential sites of intense hydrothermal degassing. Calderas on Earth occasionally become restless in what is referred to as a caldera unrest[51,52]. In addition to ground uplift and heightened seismicity, commonly observed signs of caldera unrest include macroscopic changes in hydrothermal degassing (*e.g.*, enlarging of exhaling zones and increasing volatile fluxes) and more subtle compositional changes in surface hydrothermal manifestations, whose detection and interpretation requires careful scrutiny by volcano geochemists[29,28,53,54]. However, manifestations (fumaroles, soils, mud pools, groundwaters) normally targeted by research/monitoring[55,56] are typically limited to the emerged (subaerial) portions of calderas, leaving their offshore sectors frequently unexplored. At calderas that are in (large) part submerged (for example, roughly one third of the CFc lies underwater; Fig. 1), ignoring hydrothermal venting on the seafloor can cause a (potentially severe) underestimation of caldera degassing, eventually also limiting our ability to fully capture dynamics and temporal evolution of unrest.

Our results here (Figs. 2, 3) indicate that large portions of the CFc offshore are characterized by above-atmospheric pCO_2 values (Fig. 5). In the 5 high pCO_2 zones described above (see results), vigorous bubbling activity is visible, both on the seafloor and at the air-seawater interface. These results suggest

that the venting of CO_2-rich fluids is recurrent and widespread in several segments of the submerged CFc offshore. We anticipate that submarine hydrothermal venting may be a recurrent process at many (most) partly to totally submerged calderas worldwide. Caldera-hosted degassing systems span different geodynamic settings, and a wide spectrum of depths and environmental contexts, from shallow tropical coral reefs, subtropical and temperate nearshore habitats – including sandy bottoms, seagrasses, and algal rocky reefs[4–7,57,58] – to deepsea arc/back-arc calderas like those in the Tonga-Kermadec, Eolian Islands and the Mariana arcs[59–61]. This environmental heterogeneity highlights that submarine calderas can influence diverse marine ecosystems across latitudes and settings, with implications of caldera degassing extending well beyond any single site. The diversity of emission forms and environments makes extrapolation of the few available data very difficult. Hence, the global CO_2 output from this form of volcanic degassing, which is missing from current inventories[62–65], needs to be quantified by the implementation of a more systematic and widespread observational program.

A structural control on CO_2 seafloor discharge. The seawater observations here, integrated with previous results for the groundwater system inland[32], allow a system-wide mapping of CO_2 degassing that includes both the CFc onshore and offshore (Fig. 4). This is the first map of its kind at an active caldera (at least to our knowledge), and offers a more complete view of CO_2 degassing extents and pathways at CFc than possible with terrestrial observations alone.

In the central, eastern portion of the map, we identify an overall land-to-sea continuity in high CO_2 degassing in a sector (sector 1 in Fig 4a) that extends from Pozzuoli-Agnano-Bagnoli inland to their adjacent offshores. This large high-CO_2 anomaly is centered on, but wider than, the Solfatara crater[66], a tuff cone/maar-diatreme structure[67,68] formed circa 3.9 ka BP, and representing the largest diffuse degassing structure in the CFc[28,31,69]. Our results here (Fig. 4) indicate that the CO_2 anomaly not only extends west (toward Pozzuoli), north (toward Astroni crater), east (Bagnoli) and north-east (Agnano) of Solfatara crater, as previously noted[32], but also to the south in the Bagnoli-Accademia offshore (Fig. 3-4). It is also worth noting that the seawater CO_2 anomaly, stretching from Accademia to Bagnoli (Fig. 3a and 4), roughly corresponds to the area where an incipient fault system[70], where more than 50% of the post-2022 seismicity is thought to have been concentrated (Fig. 1,4), would intersect the seafloor (Fig. 4b). The Accademia geodetic anomaly[71], an area of reduced (slower) uplift that manifested since 2021, causing a local deviation from the typical bell-shaped deformation pattern, is located north-northwest of this area. We hence interpret the Pozzuoli-Accademia-Bagnoli seawater anomaly as due to a combination of (i) direct CO_2 contribution from the incipient fault system and surrounding highly fractured zones, affected by recurrent seismicity, and (ii) discharge into seawater of CO_2-rich aqueous fluids delivered by the aquifer system inland (Fig 4b). This latter process is perhaps also responsible for the seawater pCO_2 anomaly in the Baia Castle beach area (Fig. 2), where groundwaters in the adjacent inland sector are similarly CO_2-rich (sector 2 in Fig 4a).

In addition to delimiting the extension into seawater of previously known anomalous CO_2 degassing zones (sectors 1 and 2 above), our results also identify areas (sectors 3-5) of degassing that would otherwise have escaped detection from terrestrial observations alone.

Our caldera-wide survey identifies the SdF CO_2 plume well (Fig. 2, 3). Hydrothermal venting of CO_2-rich fluids[44] at SdF has been known for centuries[72], and the CO_2/heat output from this manifestation has already been characterized in a dedicated study[33]. Our map here (Fig. 4) indicates that the SdF CO_2 anomaly is in correspondence with trending faults that have been active[73,24,27,74] during the ongoing unrest (see Fig. 4b) and before/during the Monte Nuovo eruption, when this fault system fed the eruptive vent[33,75], destroying part of the Roman structures[34]. These N-S faults are part of a wider fault system in the caldera offshore[27] that correspond to the bordering faults of the caldera resurgent block[39]. Vigorous CO_2 venting at SdF confirms that this fault system is still active. It is therefore likely that the southern segment of the resurgent block bordering faults, not investigated in this study (seawater depth extends to more than -80 m), is also affected by active hydrothermal venting.

Finally, the high CO_2 anomalies in the Nisida and Capo Miseno areas (sectors 4 and 5 in Fig. 4a) are found at the seawater intersection of the outer caldera rim bordering faults. These faults formed during the 15 ka old Tufo Giallo Napoletano (TFG) caldera-forming eruption[76]. However, at both Nisida and Capo Miseno, these caldera rims are home to eruptive vents that were active at the end of the third epoch of the CF volcanism. Hence, although volcanism at CFc has mainly clustered in the caldera center during the last 5.5 ka[77], our results suggest that the caldera outer bordering faults may be degassing and active more than groundwater results inland would suggest.

Caldera-scale submarine CO_2 degassing: significant or marginal? Our results set the basis for a first, very preliminary quantification of the total CO_2 output sustained by the CFc offshore. To this aim, we rely upon the pCO_2 results illustrated in the cross-section of Fig. 3b that, stretching in a ESE-WNW direction across the Pozzuoli bay, is roughly perpendicular to the dominant NE-SW seawater current direction (see below, Supplementary Figure 6).

We initially use a software[78] specifically designed to solve the seawater carbon system to convert the pCO_2 values (of Fig. 3a; range, 423-8029 µatm) into Total Dissolved Inorganic Carbon (TDIC). Calculations are run using average salinity, temperature and alkalinity of respectively 37.9‰, 19.7 °C and 2600 µmol/kg, and output TDIC values of 2280-2830 µmol/kg.

Next, to quantify the TDIC contribution related to hydrothermal seepage, the background (ambient) seawater TDIC must be subtracted. This includes any atmospheric and biogenic carbon contribution to the seawater system. Our pCO_2 population is manifestly polimodal (Fig. 5), and is best fit (AIC, Akaike Information Criterion: $6.47 \cdot 10^3$; Bayesian Information Criterion, BIC: $6.51 \cdot 10^3$) by a mixture of 3 sub-

populations each with gaussian distributions. The dominant population, accounting for 84.7% of the dataset, has a mean pCO_2 of 484 µatm, and is interpreted as representative of ambient background seawater (Fig. 5); while populations 2 and 3, accounting for 12.9% and 2.4% of the dataset, are interpreted as reflecting above background pCO_2 levels in far-from-hydrothermal seep (e.g., at the margin of bubbling areas) and close-to-hydrothermal seep (at and above bubbling areas) environments, respectively (see Fig. 5). The mean pCO_2 of these two sub-populations are 753 and 2770 µatm, respectively. Hence, subtracting a background seawater TDIC of 2297 µmol/kg (corresponding to a pCO_2 of a 484 µatm), the TDIC calculated above (2280-2830 µmol/kg) convert into Excess (above background seawater) Dissolved Carbon ($TDIC_{excess}$) contents of 0 to 534 µmol/kg. We interpolate and integrate such $TDIC_{excess}$ results across the whole cross-sectional area AA' of Fig. 3b, using a Sequential Gaussian Simulation[79], to obtain an integrated Excess Carbon content of 2.7±0.03 mol·m^2/kg.

Finally, we estimate the advective transport of Excess Carbon across transect AA' using seawater current velocities derived from an ocean circulation model for the Baia–Bagnoli area (see Methods and Fig. S6). The vertical profile of the normal velocity $vn\,(z)$ and the associated transport $Q\,(z)$ reveal a clear two-layer circulation (Fig. S6a), with net inflow in the upper water column and compensating outflow at depth. Considering that the maximum depth of section AA' is ~15 m, we here rely on velocity results for the upper layer, in which the mean current velocity is estimated at −0.0041 ± 0.0121 m/s (Fig. S6a). The negative mean value obtained, and its large associated standard deviation, concur to indicate that a weak (but temporally variable) water inflow toward the gulf prevails. For comparison, the mean velocity at surface (0 m) returned by the circulation model is a factor circa 2 higher (−0.0076 ± 0.021 m/s; Fig. S6b). Combining these velocities with the integrated Excess Carbon content (2.7 ± 0.03 mol·m²/kg), the Excess Carbon flux is estimated at 11.3 mol/s (≈ 43.1 tons CO_2/day) using the upper-layer mean velocity (0.0041 m/s), and 21.1 mol/s (≈ 80.4 tons CO_2/day) when the model-derived surface velocity (0.0076 m/s) is considered instead. It is important to keep in mind that the relatively low mean current velocities inferred above are partially a result of the coexistence of negative (landward current flow) and positive (seaward current flow) values. If we consider for example the upper range ranges of landward (−0.0286 m/s) and seaward (+0.0134 m/s) surface velocities, the excess CO_2 flux would increase to 302 tons and 141 tons CO_2/day, respectively. Similar results (fluxes ranging between 84 and 170 tons CO_2/day) would be obtained using the full velocity range across the water column in the 0-15m vertical profile (Fig. S6a). Overall, these results suggest that the advective CO_2 transport across the section falls within the 43–302 tons CO_2/day range.

Our calculations above have large associated uncertainties. For example, the ocean circulation model simulations used for our flux estimations robustly reproduce the overall circulation pattern within the basin and provide, to our knowledge, the most comprehensive state-of-the-art characterization currently available for this area. However, although the model horizontal resolution is sufficient to resolve the

main coastal circulation patterns, some submesoscale processes and nearshore shear may remain partially unresolved. This limitation may introduce moderate biases in pointwise velocity estimates, likely leading to a slight underestimation of local velocity extremes. Nevertheless, the maximum simulated velocities (of about 0.1 m/s) are consistent with the range reported from ADCP (Acoustic Doppler Current Profiler) and drifter observations in the Bagnoli–Coroglio Bay within the Gulf of Pozzuoli[80], providing confidence in our results, and supporting the overall reliability of the model in representing the magnitude and structure of the circulation within the Gulf of Pozzuoli.

We also caution that the quality of our calculations is limited by the small density of our observation points (see Fig. 1) that renders the extrapolation and integration procedure highly inaccurate. We cannot exclude, or even consider likely, that other substantial emission zones exist in the bay that may have been missed by our sparse observations. Conversely, we cannot exclude that our sampling grid is somewhat biased by oversampling emission zones with visible surface manifestations (e.g., known areas of bubble emission). We hence advise our calculations are only to be viewed as an order of magnitude assessment of the CO_2 flux.

With these limitations in mind, we note our inferred CO_2 flux range (43–302 tons/day) for the submerged CFc sector corresponds to circa 1.4-10% of the CO_2 flux from the Solfatara Diffuse Degassing Structure (CO_2 flux of ~3000 tons/day), the main degassing structure in the caldera onshore[45,31,28,81]. This strongly exhaling area, centered on the Solfatara tuff crater[67,68] (Fig. 1, 4), has been the primary target of geochemical monitoring so far[28]. While emphasising that additional measurements - with a denser observation grid - are required for a refined CO_2 flux assessment, our results here suggest that while CO_2 degassing today predominantly occurs in the inland CFc sector, the caldera offshore is a non-trivial source of CO_2. More effective integration of the submerged caldera sector in ongoing geochemical volcano monitoring efforts is hence recommended.

Impact of CO_2 degassing on microbial diversity. The widespread and structurally controlled release of CO_2-rich fluids documented across the submerged sector of the Campi Flegrei caldera (Fig. 2) exerts a first-order control on the chemical and biological organization of the overlying microbial diversity, with potential impacts on the entire gulf marine ecosystem. Rather than representing a perturbation, CO_2 degassing generates sharp and persistent geochemical gradients in the seawater column (Fig. 3), locally modifying pH, dissolved inorganic carbon availability, redox conditions, and, as expected from studies from other shallow water hydrothermal vents worldwide[82,83], influencing the delivery of reduced compounds and trace metals. Together, these factors define a mosaic of highly heterogeneous microenvironments that act as ecosystem engineers, selecting for specific metabolic strategies and structuring microbial communities over spatial scales ranging from centimeters to hundreds of meters[10,13,84].

Our results on the microbial diversity show that active degassing areas host dense and functionally distinct microbial assemblages dominated by chemolithoautotrophic and mixotrophic lineages, particularly within vent fluids and associated biofilms (Fig. 6). These communities are enriched in metabolic pathways linked to carbon fixation and sulfur cycling that are characteristic of hydrothermal systems (Fig. 8), including the reductive tricarboxylic acid cycle and the Wood–Ljungdahl pathway, alongside more broadly distributed pathways such as the Calvin–Benson–Bassham cycle. Importantly, these functional signatures are not confined to the immediate vent environment. Instead, genes and taxa typically associated with hydrothermal activity are detectable—albeit at much lower relative abundance—in the surrounding seawater column, with systematic gradients linked to depth, distance from the vent, and local pH (Fig. 6, 7 and 8). This pattern is consistent with dilution and mixing of hydrothermal plumes into ambient seawater, indicating that CO_2 degassing sites act as conduits exporting subsurface-derived microorganisms and metabolic potential into the coastal ocean[85,86]. This is in line with early reports of subsurface microorganisms venting from deep sea hydrothermal vents[87], and later studies using venting sites as windows to study the subsurface biosphere[88–90].

While our data do not allow quantification of *in situ* carbon fixation rates, the observed functional imprint strongly suggests that CO_2 degassing may locally enhance microbial primary productivity by increasing carbon availability and sustaining redox disequilibria. Hydrothermal fluids at Campi Flegrei are known to transport not only CO_2 but also reduced sulfur species, iron, and other trace metals[33,44], which can further stimulate chemolithotrophic metabolism and relieve micronutrient limitations in coastal waters. Similar coupling between volcanic CO_2 release, metal enrichment, and elevated microbial productivity has been reported in other shallow-water hydrothermal systems and natural CO_2 seeps[91,92], supporting the interpretation that degassing-driven inputs can subsidize local biogeochemical cycling rather than simply imposing stress. In this context, CO_2 acts not in isolation but as part of a broader geochemical package that reshapes the metabolic landscape of the ecosystem.

At the same time, the ecological consequences of CO_2 degassing are inherently scale- and taxa-dependent (Fig. 6 and 7), and might affect meiofauna and macroorganism differently[93,94]. The extreme pH conditions measured near active vents are expected to impose strong physiological constraints on many eukaryotic organisms and higher trophic levels, consistent with observations from other acidified volcanic settings[95,96]. These stress effects are likely to result in localized exclusion or reduced performance of sensitive taxa[97,98]. However, for microorganisms, the conditions documented here impose a forcing on the community composition selecting for taxa capable to exploit hydrothermal conditions, rather than constituting a stressor for mesophilic, background condition adapted communities. Our data indicate that microbial communities respond primarily through compositional and functional reorganization, with shifts toward metabolisms capable of exploiting elevated CO_2 concentrations, reduced compounds, and metal availability. Thus, CO_2 degassing simultaneously

generates zones of ecological stress for some components of the ecosystem, mainly meiofauna and macrofauna as extensively documented in the literature[99,100] and zones of enhanced opportunity for microorganisms[8,15], reinforcing the view of volcanic degassing as a driver of ecological diversity. Additionally, microorganisms present on the seafloor and in the shallow crust and active within the hydrothermal system might contribute to alter the composition and quantity of volatiles recycled to the surface as previously reported for other volcanic degassing areas[16–18], possibly further limiting our estimates of CO_2 released to the water column and atmosphere.

More broadly, the Campi Flegrei exemplifies how submerged calderas can function as persistent interfaces between the deep Earth and the ocean, coupling magmatic degassing, subsurface microbial ecosystems, and coastal marine biogeochemistry. The export of hydrothermal microorganisms and functions into the water column implies a previously underappreciated pathway by which the subsurface biosphere can influence nearshore ecosystems. In addition, the net export of CO_2, nutrients and trace metals from the venting area to the surrounding environments as exemplified by the detected pCO_2 plumes has the potential to fertilize primary productivity with positive cascading effects on the local coastal diversity[101,102]. Trace metals released from water rock interactions might be particularly important in controlling biogeochemical cycles in the surrounding areas[103,104] by altering the available metabolic pathways available to microorganisms[105]. Given the abundance of partially or fully submerged calderas worldwide, similar processes are likely to operate far beyond Campi Flegrei, with implications for regional carbon cycling, nutrient dynamics, and ecosystem structure that are not captured by studies focused solely on subaerial degassing or open-ocean hydrothermal systems.

Taken together, our results show that submarine CO_2 degassing in underwater calderas is not merely a geochemical expression of volcanic unrest, but a dynamic ecological force capable of reorganizing microbial community structure and function at large scales influencing surrounding ecosystems. Integrating biological observations with high-resolution degassing surveys reveals submerged calderas as active biogeochemical reactors, where Earth processes and marine ecosystems are tightly and continuously coupled.

Methods

pCO_2 underwater sensors. The seawater results from the Pozzuoli Bay were obtained during nine different surveys performed from June 2023 to November 2025 using appropriate underwater CO_2 sensors: the HydroC™ CONTROS System and Solutions (Kiel, Germany) and the CO2-Pro™ OCEANUS CV Submersible pCO2 Sensor. Both sensors are compact submersible systems developed for *in situ* determination of the partial pressure of carbon dioxide (pCO_2) in seawater. Their analytical principle is based on nondispersive infrared (NDIR) spectrometry, whereby dissolved CO_2 permeates a gas-permeable membrane into an internal equilibration volume[33,106]. Continuous flushing of the

membrane surface is ensured by an external pump, which both supplies seawater to the sensor head and minimizes boundary layer effects that could otherwise impair diffusion rate[106]. Data acquisition was carried out at a frequency of 1 Hz and transmitted in real time to a computer via a 50 m communication cable. The HydroC™ CONTROS System was calibrated across a temperature range of 13–30 °C, with a working pCO_2 interval between 100 and 6000 µatm (10–600 Pa). Measurement precision is better than 1 µatm (0.1 Pa). To mitigate instrumental drift, the sensor was operated with regular automated sequences consisting of 120s zeroing intervals and 480s flushing phases, the results of which were applied during subsequent calibration correction[106]. The characteristic response time (T_{63}) was determined to be 20 ± 2s near the surface and approximately 30s at ~20 m depth. CO2-Pro™ OCEANUS CV Submersible pCO_2 Sensor was designed to accommodate a broader concentration spectrum—from nominal ranges (e.g., 0–600 ppm) up to 10 000 ppm and was used in the areas were the pCO_2 exceeded the 2000 µatm. The instrument's measurement is underpinned by high accuracy (±0.5%) and a fine resolution of 0.01 ppm, enhanced through automatic zero compensation and factory calibration using WMO-traceable (World Meteorological Organization) standards gases for long-term stability. Equilibration time (t_{63}) was approximately 50 seconds with a pumped head at 20 °C, yielding rapid sensor responsiveness under flow conditions.

Seawater vertical profiles were obtained along a relatively regular grid with a spacing between 100-200m, particularly, in the areas where pCO_2 was relatively low (close to the normal seawater value ~400-500 µatm[43]). During each survey, vertical profiles, far from the hydrothermal areas, were acquired in order to check the local seawater background. The spacing was reduced (10 – 50m) near hydrothermal vents (e.g., Secca delle Fumose, Baia Castle beach, Academia-Bagnoli-Nisida coast and Capo Miseno area). A total of 273 geochemical profiles were performed covering an area of approximately ~19 km^2. At each site, the CO_2 sensor was lowered from a small boat down to the seafloor, and then raised up to the seawater surface at a rate of 20cm/s. While performing the measurements along each vertical profile, and at each 4-5m step, the CO_2 sensor was stopped and maintained at a constant depth for a few minutes (2-3), in order to allow the sensors to fully equilibrate. After equilibration and based on the depth of the seafloor, we measured the pCO_2 at 1 (0-4m), 2 (4-8m) or 3 (8-15m) different depths for each profile. Finally, given the irregularity of the seafloor in the areas of Secca delle Fumose and Capo Miseno, the vertical profiling was assisted by a scuba diver to ensure that the sensors measured the pCO_2 near-vent plumes.

The final maps were developed using the maximum pCO_2 registered at each depth. Spatial interpolation and mapping (Figs. 2-3) were performed in Surfer® (from Golden Software, LLC; www.goldensoftware.com[107]) using ordinary kriging, a geostatistical interpolation method that explicitly models spatial autocorrelation; empirical semivariograms were computed and fitted with a theoretical model, which was then used to estimate values at unsampled locations and generate

continuous spatial maps. Semivariogram parameters (nugget, sill, and range) were estimated by weighted least squares, and kriging predictions were computed on a regular grid covering the study area.

Seawater pCO_2 profiles (Fig. 3) were generated using the Data-Interpolating Variational Analysis (DIVA) gridding method implemented in Ocean Data View (ODV)[108]. DIVA variational interpolation technique produces spatially consistent fields by minimizing a cost function constrained by data misfit and smoothness; in this study, gridded pCO_2 values were extracted along the vertical dimension to obtain continuous profiles. DIVA gridding was applied using default ODV parameters, with correlation length scales and signal-to-noise ratios optimized internally by the software. The resulting three-dimensional gridded fields were used to derive vertical seawater pCO_2 profiles.

Modelling sea water current in the Pozzuoli bay. Surface and subsurface currents in the Gulf of Pozzuoli were estimated using a high-resolution regional ocean hindcasts of the Gulf of Naples for 2016 based on the Coastal Regional Ocean Model (CROM)[109]. The model domain (40°–41.43° N, 13°–15.36° E) was implemented on a regular grid with horizontal resolution of ≈ 600 m and 40 terrain-following sigma levels, with the bathymetry derived from the 30″ GEBCO dataset. Initial and open-boundary conditions consistent with the basin-scale transports were guaranteed through the one-way nesting[110] within the Mediterranean NEMO-OPA circulation model[111]. Surface boundary conditions, i.e. momentum from wind, heat and freshwater fluxes, were computed from the 5-km resolution SKIRON/Eta atmospheric model at a temporal step of 6 hours. The simulation consisted of twelve monthly hindcasts for the year analysed, with monthly re-initialisation using satellite-derived sea surface temperature (SST) provided by the Copernicus Marine Environment Monitoring Service (CMEMS) to constrain the surface heat fluxes[112]. Every simulation was initialized one week prior to the target month to allow model adjustment, so that the outputs of the first six days were discarded to remove potential initialisation transients associated with the spin-up phase.

Volume transport across the AA' transect was computed by integrating the velocity component normal to the section across the full water column:

$$Q = \sum_{k,s} v_n(k,s)\, A(k,s) \tag{1}$$

where vn is the velocity component normal to the section and A(k,s) is the cross-sectional area associated with each grid segment and sigma layer. Land points were excluded from the calculation.

Biological samples collection. Biofilm samples and hydrothermal fluids were collected by divers at both hot, focused and warm, diffuse venting sites, minimizing disturbance of the sampled matrices. Seawater column samples were collected from the vessel using Niskin bottles following a depth-stratified approach: (i) a single depth when seafloor depth was <6 m below seafloor (bsf); (ii) two depths when seafloor depth ranged between 6 and 8 m bsf; and (iii) three depths when seafloor depth exceeded 8 m bsf. The maximum sampling depth was 15 m bsf. In total, 27 samples were collected for biological analyses, including biofilms (n = 5), hydrothermal fluid (n = 1), and seawater (n = 21). Samples SF1D13_B1 and SF1D13_B2 correspond to orange biofilms collected directly at the SdF emission site in June and July 2023, respectively. Samples SF2A_B1, SF2B_B1, and SF2C_B1 correspond to white biofilms collected from colder seafloor areas characterized by diffuse hydrothermal venting. Sample SF1D13_F2 represents the hydrothermal fluid collected at the SdF emission site. Seawater samples (TxDy) were collected from the water column surrounding SdF at distinct transect sites and depths (x = transect site; y = depth; Fig. 2b). Hydrothermal fluid and seawater samples were filtered in the field through 0.22 µm Sterivex filter membranes for biomass concentration. Biofilm samples from the SdF vent and surrounding venting seafloor were collected in sterile 50-mL centrifuge tubes. In the laboratory, Sterivex filters and biofilm samples were stored at −20 °C until DNA extraction. Physico-chemical parameters of fluids were measured *in situ* using a multiparametric probe (HANNA, HI98494). Fluid aliquots were filtered through 0.22 µm membranes for immediate determination of total alkalinity.

DNA extraction and shotgun metagenomics. DNA was extracted from Sterivex filters and biofilm samples using a modified phenol–chloroform extraction protocol optimized for shallow-water hydrothermal vents and seawater samples[10]. DNA concentration was quantified fluorometrically using a Qubit (Thermo Fisher Scientific). Shotgun metagenomic sequencing was performed at Novogene with the NExtSeq Illumina platform (PE 2x150) with a sequencing depth between 15 and 30 million reads per sample.

Bioinformatic and statistical analysis. Raw shotgun metagenomic reads were processed using the GeoMosaic pipeline (Giovannelli Lab, https://giovannellilab.github.io/Geomosaic/index.html), which performs integrated quality control, taxonomic profiling, functional annotation, and metagenome assembly. Sequencing reads were first quality-filtered and trimmed within GeoMosaic using Fastp, Fastqc and Reads Count; then, high-quality reads were functionally annotated using Kaiju, employing a protein-level classification strategy suitable for hydrothermal vent and marine metagenomes[113–115]. Functional annotation of the same reads was carried out using FunProfiler together with a custom database of KEGG orthologues (KOs) associated with biogeochemical cycles[116]. Diversity analyses were conducted in R using the *phyloseq* package within a Jupyter notebook instance[117]. Beta diversity

was evaluated using weighted Jaccard distance metrics, as implemented in the vegan package[118]. All statistical analyses and visualizations were performed in R v4.5.1 (R Core Team, 2021) using *ggplot2*[119].

Data availability

The datasets generated and/or analyzed during the current study are available in the Supplementary Tables provided with this manuscript. All sequencing data generated in this study, including 16S rRNA gene amplicons and shotgun metagenomes, have been deposited in the European Nucleotide Archive (ENA) under the project accession number PRJEB87249 under the Umbrella Project CoEvolve PRJEB55081. Sequences from the Barosa et al. (2025) study are available under access number PRJEB67762 under the same Umbrella Project. The bioinformatic code used for data processing and analysis, together with associated metadata files, is publicly available in the GitHub repository https://github.com/giovannellilab/Sandoval-Velasquez_Campi_Flegrei_degassing/tree/main and archived on Zenodo under DOI 10.5281/zenodo.18800558.

References

1. Branney, M. & Acocella, V. Calderas. in *The Encyclopedia of Volcanoes* 299–315 (Elsevier, 2015). doi:10.1016/B978-0-12-385938-9.00016-X.
2. Rouwet, D. *Volcanic Lakes*. (Springer Berlin / Heidelberg, Berlin, Heidelberg, 2015).
3. Fouquet, Y. *et al.* Volcanic and hydrothermal processes in submarine calderas: The Kulo Lasi example (SW Pacific). *Ore Geol. Rev.* **99**, 314–343 (2018).
4. Enochs, I. C. *et al.* Shift from coral to macroalgae dominance on a volcanically acidified reef. *Nat. Clim. Change* **5**, 1083–1088 (2015).
5. Tarasov, V. G. *et al.* Effect of shallow-water hydrothermal venting on the biota of Matupi Harbour (Rabaul Caldera, New Britain Island, Papua New Guinea). *Cont. Shelf Res.* **19**, 79–116 (1999).
6. Aiuppa, A. *et al.* Volcanic CO2 seep geochemistry and use in understanding ocean acidification. *Biogeochemistry* **152**, 93–115 (2021).
7. Agostini, S. *et al.* Geochemistry of two shallow CO2 seeps in Shikine Island (Japan) and their potential for ocean acidification research. *Reg. Stud. Mar. Sci.* **2**, 45–53 (2015).
8. Price, R. E. & Giovannelli, D. A Review of the Geochemistry and Microbiology of Marine Shallow-Water Hydrothermal Vents. in *Reference Module in Earth Systems and Environmental Sciences* B9780124095489095233 (Elsevier, 2017). doi:10.1016/B978-0-12-409548-9.09523-3.
9. Sievert, S. & Vetriani, C. Chemoautotrophy at Deep-Sea Vents: Past, Present, and Future. *Oceanography* **25**, 218–233 (2012).
10. Giovannelli, D., d'Errico, G., Manini, E., Yakimov, M. & Vetriani, C. Diversity and phylogenetic analyses of bacteria from a shallow-water hydrothermal vent in Milos island (Greece). *Front. Microbiol.* **4**, (2013).
11. Barosa, B. *et al.* Mapping the microbial diversity associated with different geochemical regimes in the shallow-water hydrothermal vents of the Aeolian archipelago, Italy. *Front. Microbiol.* **14**, 1134114 (2023).
12. Barosa, B. *et al.* The microbiology and geochemistry of the shallow-water hydrothermal vents of the Gulf of Naples, Italy. Preprint at https://doi.org/10.1101/2025.10.02.679971 (2025).
13. Yücel, M. *et al.* Eco-geochemical dynamics of a shallow-water hydrothermal vent system at Milos Island, Aegean Sea (Eastern Mediterranean). *Chem. Geol.* **356**, 11–20 (2013).

14. Gomez-Saez, G. V. *et al.* Relative Importance of Chemoautotrophy for Primary Production in a Light Exposed Marine Shallow Hydrothermal System. *Front. Microbiol.* **8**, 702 (2017).
15. Giovannelli, D. & Price, R. E. Marine Shallow-Water Hydrothermal Vents: Microbiology. in *Encyclopedia of Ocean Sciences* 353–363 (Elsevier, 2019). doi:10.1016/B978-0-12-409548-9.11250-3.
16. Barry, P. H. *et al.* Forearc carbon sink reduces long-term volatile recycling into the mantle. *Nature* **568**, 487–492 (2019).
17. Fullerton, K. M. *et al.* Effect of tectonic processes on biosphere-geosphere feedbacks across a convergent margin. *Nat. Geosci.* **14**, 301–306 (2021).
18. Giovannelli, D. *et al.* Subsurface life can modify volatile cycling on a planetary scale. *Mem. Della Soc. Astron. Ital.* **92**, 60–63 (2021).
19. Del Gaudio, C., Aquino, I., Ricciardi, G. P., Ricco, C. & Scandone, R. Unrest episodes at Campi Flegrei: A reconstruction of vertical ground movements during 1905–2009. *J. Volcanol. Geotherm. Res.* **195**, 48–56 (2010).
20. Scarpa, R. *et al.* Historic Unrest of the Campi Flegrei Caldera, Italy. in *Campi Flegrei* (eds Orsi, G., D'Antonio, M. & Civetta, L.) 257–282 (Springer Berlin Heidelberg, Berlin, Heidelberg, 2022). doi:10.1007/978-3-642-37060-1_10.
21. Kilburn, C. R. J., Carlino, S., Danesi, S. & Pino, N. A. Potential for rupture before eruption at Campi Flegrei caldera, Southern Italy. *Commun. Earth Environ.* **4**, 190 (2023).
22. Astort, A. *et al.* Tracking the 2007–2023 magma-driven unrest at Campi Flegrei caldera (Italy). *Commun. Earth Environ.* **5**, 506 (2024).
23. Orsi, G. *et al.* Short-term ground deformations and seismicity in the resurgent Campi Flegrei caldera (Italy): an example of active block-resurgence in a densely populated area. *J. Volcanol. Geotherm. Res.* **91**, 415–451 (1999).
24. Tramelli, A., Convertito, V. & Godano, C. b value enlightens different rheological behaviour in Campi Flegrei caldera. *Commun. Earth Environ.* **5**, 275 (2024).
25. Scotto Di Uccio, F. *et al.* Delineation and Fine-Scale Structure of Fault Zones Activated During the 2014–2024 Unrest at the Campi Flegrei Caldera (Southern Italy) From High-Precision Earthquake Locations. *Geophys. Res. Lett.* **51**, e2023GL107680 (2024).
26. De Landro, G. *et al.* 3D structure and dynamics of Campi Flegrei enhance multi-hazard assessment. *Nat. Commun.* **16**, 4814 (2025).
27. Tan, X. *et al.* A clearer view of the current phase of unrest at Campi Flegrei caldera. *Science* **390**, 70–75 (2025).
28. Chiodini, G. *et al.* The Hydrothermal System of the Campi Flegrei Caldera, Italy. in *Campi Flegrei* (eds Orsi, G., D'Antonio, M. & Civetta, L.) 239–255 (Springer Berlin Heidelberg, Berlin, Heidelberg, 2022). doi:10.1007/978-3-642-37060-1_9.
29. Chiodini, G. *et al.* Magmas near the critical degassing pressure drive volcanic unrest towards a critical state. *Nat. Commun.* **7**, 13712 (2016).
30. Caliro, S. *et al.* Escalation of caldera unrest indicated by increasing emission of isotopically light sulfur. *Nat. Geosci.* **18**, 167–174 (2025a).
31. Cardellini, C. *et al.* Monitoring diffuse volcanic degassing during volcanic unrests: the case of Campi Flegrei (Italy). *Sci. Rep.* **7**, 6757 (2017).
32. Caliro, S. *et al.* Chemical and isotopic characterization of groundwater and thermal waters from the Campi Flegrei caldera (southern Italy). *J. Volcanol. Geotherm. Res.* **460**, 108280 (2025b).
33. Di Napoli, R. *et al.* Hydrothermal fluid venting in the offshore sector of C ampi F legrei caldera: A geochemical, geophysical, and volcanological study. *Geochem. Geophys. Geosystems* **17**, 4153–4178 (2016).
34. Passaro, S. *et al.* Multi-resolution morpho-bathymetric survey results at the Pozzuoli–Baia underwater archaeological site (Naples, Italy). *J. Archaeol. Sci.* **40**, 1268–1278 (2013).
35. Natale, J. *et al.* Integrated on-land-offshore stratigraphy of the Campi Flegrei caldera: New insights into the volcano-tectonic evolution in the last 15 kyr. *Basin Res.* **34**, 855–882 (2022a).
36. Natale, J. *et al.* Fault systems in the offshore sector of the Campi Flegrei caldera (southern Italy): Implications for nested caldera structure, resurgent dome, and volcano-tectonic evolution. *J. Struct. Geol.* **163**, 104723 (2022b).

673 37. Steinmann, L., Spiess, V. & Sacchi, M. The Campi Flegrei caldera (Italy): Formation and
674 evolution in interplay with sea-level variations since the Campanian Ignimbrite eruption at 39 ka. *J.*
675 *Volcanol. Geotherm. Res.* **327**, 361–374 (2016).
676 38. Steinmann, L., Spiess, V. & Sacchi, M. Post-collapse evolution of a coastal caldera system:
677 Insights from a 3D multichannel seismic survey from the Campi Flegrei caldera (Italy). *J. Volcanol.*
678 *Geotherm. Res.* **349**, 83–98 (2018).
679 39. Sacchi, M. *et al.* The Neapolitan Yellow Tuff caldera offshore the Campi Flegrei: Stratal
680 architecture and kinematic reconstruction during the last 15ky. *Mar. Geol.* **354**, 15–33 (2014).
681 40. Aucelli, P., Cinque, A., Mattei, G., Pappone, G. & Rizzo, A. Studying relative sea level change
682 and correlative adaptation of coastal structures on submerged Roman time ruins nearby Naples
683 (southern Italy). *Quat. Int.* **501**, 328–348 (2019).
684 41. Aucelli, P. P. C. *et al.* Multi-proxy analysis of relative sea-level and paleoshoreline changes during
685 the last 2300 years in the Campi Flegrei caldera, Southern Italy. *Quat. Int.* **602**, 110–130 (2021).
686 42. Baldrighi, E. *et al.* Meiofaunal communities and nematode diversity characterizing the Secca delle
687 Fumose shallow vent area (Gulf of Naples, Italy). *PeerJ* **8**, e9058 (2020).
688 43. Berry. The impact of human CO2 on atmospheric CO2. *Sci. Clim. Change Int. J. Sci. Philos.* 36
689 (2022) doi:10.53234/scc202112/212.
690 44. Vaselli, O., Franco, T., Dario, T., Robert, P. J. & Antonio, C. Submarine and Inland Gas
691 Discharges from the Campi Flegrei (Southern Italy) and the Pozzuoli Bay: Geochemical Clues for
692 a Common Hydrothermal-Magmatic Source. *Procedia Earth Planet. Sci.* **4**, 57–73 (2011).
693 45. Buono, G., Caliro, S., Paonita, A., Pappalardo, L. & Chiodini, G. Discriminating carbon dioxide
694 sources during volcanic unrest: The case of Campi Flegrei caldera (Italy). *Geology* **51**, 397–401
695 (2023).
696 46. Campbell, B. J., Engel, A. S., Porter, M. L. & Takai, K. The versatile ε-proteobacteria: key players
697 in sulphidic habitats. *Nat. Rev. Microbiol.* **4**, 458–468 (2006).
698 47. Giovannelli, D. *et al.* Insight into the evolution of microbial metabolism from the deep-branching
699 bacterium, Thermovibrio ammonificans. *eLife* **6**, e18990 (2017).
700 48. Hügler, M. & Sievert, S. M. Beyond the Calvin Cycle: Autotrophic Carbon Fixation in the Ocean.
701 *Annu. Rev. Mar. Sci.* **3**, 261–289 (2011).
702 49. Pontiller, B. *et al.* Rapid bacterioplankton transcription cascades regulate organic matter utilization
703 during phytoplankton bloom progression in a coastal upwelling system. *ISME J.* **16**, 2360–2372
704 (2022).
705 50. Buchan, A., LeCleir, G. R., Gulvik, C. A. & González, J. M. Master recyclers: features and
706 functions of bacteria associated with phytoplankton blooms. *Nat. Rev. Microbiol.* **12**, 686–698
707 (2014).
708 51. Newhall, C. G. & Dzurisin, D. *Historical Unrest at Large Calderas of the World*.
709 https://pubs.usgs.gov/publication/b1855 (1988) doi:10.3133/b1855.
710 52. Acocella, V., Di Lorenzo, R., Newhall, C. & Scandone, R. An overview of recent (1988 to 2014)
711 caldera unrest: Knowledge and perspectives. *Rev. Geophys.* **53**, 896–955 (2015).
712 53. Lowenstern, J. B., Smith, R. B. & Hill, D. P. Monitoring super-volcanoes: geophysical and
713 geochemical signals at Yellowstone and other large caldera systems. *Philos. Trans. R. Soc. Math.*
714 *Phys. Eng. Sci.* **364**, 2055–2072 (2006).
715 54. Lowenstern, J. B. & Hurwitz, S. Monitoring a Supervolcano in Repose: Heat and Volatile Flux at
716 the Yellowstone Caldera. *Elements* **4**, 35–40 (2008).
717 55. Aiuppa, A., Caudron, C., Chiodini, G., Ingebritsen, S. & Viveiros, F. Geochemical Monitoring of
718 Volcanic Fluids in the Twenty-First Century. in *Modern Volcano Monitoring* (eds Spica, Z. &
719 Caudron, C.) 209–260 (Springer Nature Switzerland, Cham, 2025a). doi:10.1007/978-3-031-
720 86841-2_8.
721 56. Aiuppa, A. *et al.* Geochemical volcano monitoring. Preprint at https://doi.org/10.31223/X5TT6D
722 (2025b).
723 57. Dura, A. *et al.* The Hydrothermal Vent Field at the Eastern Edge of the Hellenic Volcanic Arc: The
724 Avyssos Caldera (Nisyros). *Geosciences* **11**, 290 (2021).
725 58. Agostini, S. *et al.* Ocean acidification drives community shifts towards simplified non-calcified
726 habitats in a subtropical−temperate transition zone. *Sci. Rep.* **8**, 11354 (2018).

59. De Ronde, C. E. J. *et al.* Submarine hydrothermal activity along the mid-Kermadec Arc, New Zealand: Large-scale effects on venting. *Geochem. Geophys. Geosystems* **8**, 2006GC001495 (2007).
60. Baker, E. T. *et al.* Hydrothermal activity and volcano distribution along the Mariana arc. *J. Geophys. Res. Solid Earth* **113**, 2007JB005423 (2008).
61. Italiano, F. & Nuccio, P. M. Geochemical investigations of submarine volcanic exhalations to the east of Panarea, Aeolian Islands, Italy. *J. Volcanol. Geotherm. Res.* **46**, 125–141 (1991).
62. Fischer, T. P. *et al.* The emissions of CO2 and other volatiles from the world's subaerial volcanoes. *Sci. Rep.* **9**, 18716 (2019).
63. Werner, C. *et al.* Carbon Dioxide Emissions from Subaerial Volcanic Regions: Two Decades in Review. in *Deep Carbon* (eds Orcutt, B. N., Daniel, I. & Dasgupta, R.) 188–236 (Cambridge University Press, 2019). doi:10.1017/9781108677950.008.
64. Fischer, T. P. & Aiuppa, A. AGU Centennial Grand Challenge: Volcanoes and Deep Carbon Global CO_2 Emissions From Subaerial Volcanism—Recent Progress and Future Challenges. *Geochem. Geophys. Geosystems* **21**, e2019GC008690 (2020).
65. Bastianoni, A. *et al.* The missing carbon budget puzzle piece: shallow-water hydrothermal vents contribution to global CO2 fluxes. Preprint at https://doi.org/10.31223/X52W81 (2022).
66. Marini, L., Principe, C. & Lelli, M. *The Solfatara Magmatic-Hydrothermal System: Geochemistry, Geothermometry and Geobarometry of Fumarolic Fluids*. (Springer International Publishing, Cham, 2022). doi:10.1007/978-3-030-98471-7.
67. Di Vito, M. A. *et al.* Volcanism and deformation since 12,000 years at the Campi Flegrei caldera (Italy). *J. Volcanol. Geotherm. Res.* **91**, 221–246 (1999).
68. Isaia, R. *et al.* Stratigraphy, structure, and volcano-tectonic evolution of Solfatara maar-diatreme (Campi Flegrei, Italy). *Geol. Soc. Am. Bull.* **127**, 1485–1504 (2015).
69. Chiodini, G. *et al.* CO_2 degassing and energy release at Solfatara volcano, Campi Flegrei, Italy. *J. Geophys. Res. Solid Earth* **106**, 16213–16221 (2001).
70. Giordano, G. *et al.* Birth and growth of a volcanotectonic fault during the current volcanic unrest at Campi Flegrei caldera (Italy). *Commun. Earth Environ.* **6**, 839 (2025).
71. Giudicepietro, F. *et al.* Burst-like swarms in the Campi Flegrei caldera accelerating unrest from 2021 to 2024. *Nat. Commun.* **16**, 1548 (2025).
72. Gianfrotta, Piero. A. Harbor Structures of the Augustan Age in Italy. in *A retrospective after Two Millennia. Atti del Convegno (Caesarea Maritima 1995)* 65–76 (Leiden-New York-Köln, 1996).
73. Scotto Di Uccio, F. *et al.* Delineation and Fine-Scale Structure of Fault Zones Activated During the 2014–2024 Unrest at the Campi Flegrei Caldera (Southern Italy) From High-Precision Earthquake Locations. *Geophys. Res. Lett.* **51**, e2023GL107680 (2024).
74. Tramelli, A., Giudicepietro, F., Ricciolino, P. & Chiodini, G. The seismicity of Campi Flegrei in the contest of an evolving long term unrest. *Sci. Rep.* **12**, 2900 (2022).
75. Di Vito, M. A. *et al.* Magma transfer at Campi Flegrei caldera (Italy) before the 1538 AD eruption. *Sci. Rep.* **6**, 32245 (2016).
76. Orsi, G., D'Antonio, M., Vita, S. D. & Gallo, G. The Neapolitan Yellow Tuff, a large-magnitude trachytic phreatoplinian eruption: eruptive dynamics, magma withdrawal and caldera collapse. *J. Volcanol. Geotherm. Res.* **53**, 275–287 (1992).
77. Orsi, G. Volcanic and Deformation History of the Campi Flegrei Volcanic Field, Italy. in *Campi Flegrei* (eds Orsi, G., D'Antonio, M. & Civetta, L.) 1–53 (Springer Berlin Heidelberg, Berlin, Heidelberg, 2022). doi:10.1007/978-3-642-37060-1_1.
78. Sharp, J. D. *et al.* CO2SYSv3 for MATLAB. Zenodo https://doi.org/10.5281/ZENODO.3950562 (2023).
79. Deutsch, C. V. & Journel, A. G. *GSLIB: Geostatistical Software Library and User's Guide*. (Oxford university press, New York, 1998).
80. Castagno, P. *et al.* Hydrographic and dynamical characterisation of the Bagnoli-Coroglio Bay (Gulf of Naples, Tyrrhenian Sea). *Chem. Ecol.* **36**, 598–618 (2020).
81. Chiodini, G. *et al.* Long-term variations of the Campi Flegrei, Italy, volcanic system as revealed by the monitoring of hydrothermal activity. *J. Geophys. Res. Solid Earth* **115**, 2008JB006258 (2010).

82. Pichler, T., Veizer, J. & Hall, G. E. M. The chemical composition of shallow-water hydrothermal fluids in Tutum Bay, Ambitle Island, Papua New Guinea and their effect on ambient seawater. *Mar. Chem.* **64**, 229–252 (1999).
83. Tarasov, V. G. Effects of Shallow-Water Hydrothermal Venting on Biological Communities of Coastal Marine Ecosystems of the Western Pacific. in *Advances in Marine Biology* vol. 50 267–421 (Elsevier, 2006).
84. Silva, A. C. P. *et al.* Tectonic setting shapes microbial biosynthetic potential across global geothermal environments. Preprint at https://doi.org/10.1101/2025.09.14.675129 (2025).
85. Dick, G. J. *et al.* The microbiology of deep-sea hydrothermal vent plumes: ecological and biogeographic linkages to seafloor and water column habitats. *Front. Microbiol.* **4**, (2013).
86. Fortunato, C. S. & Huber, J. A. Coupled RNA-SIP and metatranscriptomics of active chemolithoautotrophic communities at a deep-sea hydrothermal vent. *ISME J.* **10**, 1925–1938 (2016).
87. Deming, J. W. & Baross, J. A. Deep-sea smokers: Windows to a subsurface biosphere? *Geochim. Cosmochim. Acta* **57**, 3219–3230 (1993).
88. Giovannelli, D. *et al.* Sampling across large-scale geological gradients to study geosphere–biosphere interactions. *Front. Microbiol.* **13**, 998133 (2022).
89. Elkassas, S. M. *et al.* Metabolic and population profiles of active subseafloor autotrophs in young oceanic crust at deep-sea hydrothermal vents. *Appl. Environ. Microbiol.* **91**, e01868-25 (2025).
90. Reveillaud, J. *et al.* Subseafloor microbial communities in hydrogen-rich vent fluids from hydrothermal systems along the M id- C ayman R ise. *Environ. Microbiol.* **18**, 1970–1987 (2016).
91. Pérez-Barrancos, C. *et al.* Shallow Hydrothermal Fluids Shape Microbial Dynamics at the Tagoro Submarine Volcano (Canary Islands, Spain). *Environ. Microbiol.* **27**, e70052 (2025).
92. Gomez-Saez, G. V. *et al.* Hydrothermal iron - DOM interaction in a shallow-water hydrothermal system off Dominica Island. 2 datasets Preprint at https://doi.org/10.1594/PANGAEA.874263 (2015).
93. Bellec, L. *et al.* Microbial Communities of the Shallow-Water Hydrothermal Vent Near Naples, Italy, and Chemosynthetic Symbionts Associated With a Free-Living Marine Nematode. *Front. Microbiol.* **11**, 2023 (2020).
94. Milazzo, M. *et al.* Biogenic habitat shifts under long-term ocean acidification show nonlinear community responses and unbalanced functions of associated invertebrates. *Sci. Total Environ.* **667**, 41–48 (2019).
95. Garilli, V. *et al.* Physiological advantages of dwarfing in surviving extinctions in high-CO2 oceans. *Nat. Clim. Change* **5**, 678–682 (2015).
96. Harvey, J., König, S. & Luguet, A. The effects of melt depletion and metasomatism on highly siderophile and strongly chalcophile elements: S–Se–Te–Re–PGE systematics of peridotite xenoliths from Kilbourne Hole, New Mexico. *Geochim. Cosmochim. Acta* **166**, 210–233 (2015).
97. Hall-Spencer, J. M. *et al.* Volcanic carbon dioxide vents show ecosystem effects of ocean acidification. *Nature* **454**, 96–99 (2008).
98. Fabricius, K. E. *et al.* Losers and winners in coral reefs acclimatized to elevated carbon dioxide concentrations. *Nat. Clim. Change* **1**, 165–169 (2011).
99. Martins Medeiros, I. P. & Souza, M. M. Acid times in physiology: A systematic review of the effects of ocean acidification on calcifying invertebrates. *Environ. Res.* **231**, 116019 (2023).
100. Kroeker, K. J. *et al.* Impacts of ocean acidification on marine organisms: quantifying sensitivities and interaction with warming. *Glob. Change Biol.* **19**, 1884–1896 (2013).
101. Zhang, Z. *et al.* Substantial trace metal input from the 2022 Hunga Tonga-Hunga Ha'apai eruption into the South Pacific. *Nat. Commun.* **15**, 8986 (2024).
102. Caramanna, G., Sievert, S. M. & Bühring, S. I. Submarine Shallow-Water Fluid Emissions and Their Geomicrobiological Imprint: A Global Overview. *Front. Mar. Sci.* **8**, 727199 (2021).
103. Hay Mele, B. *et al.* Oxidoreductases and metal cofactors in the functioning of the earth. *Essays Biochem.* **67**, 653–670 (2023).
104. Giovannelli, D. Trace metal availability and the evolution of biogeochemistry. *Nat. Rev. Earth Environ.* **4**, 597–598 (2023).

105. Ricciardelli, A. *et al.* Trace metals availability controls terminal electron acceptor utilization in Escherichia coli. 2025.01.08.631794 Preprint at https://doi.org/10.1101/2025.01.08.631794 (2025).
106. Fietzek, P., Fiedler, B., Steinhoff, T. & Körtzinger, A. In situ Quality Assessment of a Novel Underwater pCO2 Sensor Based on Membrane Equilibration and NDIR Spectrometry. *J. Atmospheric Ocean. Technol.* **31**, 181–196 (2014).
107. Golden Software, L. (2025).
108. Schlitzer, R. Ocean Data View. (2024).
109. De Ruggiero, P. *et al.* Modelling the marine circulation of the Campania coastal system (Tyrrhenian Sea) for the year 2016: Analysis of the dynamics. *J. Mar. Syst.* **210**, 103388 (2020).
110. Oddo, P. *et al.* A nested Atlantic-Mediterranean Sea general circulation model for operational forecasting. *Ocean Sci.* **5**, 461–473 (2009).
111. Madec, G. & Nemo team. *NEMO Ocean Engine*. (2008).
112. Pisano, A., Buongiorno Nardelli, B., Tronconi, C. & Santoleri, R. The new Mediterranean optimally interpolated pathfinder AVHRR SST Dataset (1982–2012). *Remote Sens. Environ.* **176**, 107–116 (2016).
113. Andrews, S. FastQC: a quality control tool for high throughput sequence data. (2010).
114. Menzel, P., Ng, K. L. & Krogh, A. Fast and sensitive taxonomic classification for metagenomics with Kaiju. *Nat. Commun.* **7**, 11257 (2016).
115. Chen, S., Zhou, Y., Chen, Y. & Gu, J. fastp: an ultra-fast all-in-one FASTQ preprocessor. *Bioinformatics* **34**, i884–i890 (2018).
116. Hera, M. R. *et al.* Metagenomic functional profiling: to sketch or not to sketch? *Bioinformatics* **40**, ii165–ii173 (2024).
117. McMurdie, P. J. & Holmes, S. phyloseq: an R package for reproducible interactive analysis and graphics of microbiome census data. *PloS One* **8**, e61217 (2013).
118. Oksanen, J. *et al.* vegan: Community Ecology Package. Ordination methods, diversity analysis and other functions for community and vegetation ecologists. Version 2.4-6. URL https://CRAN.R-project.org/package=vegan. (2018).
119. Wickham, H. ggplot2. *Wiley Interdiscip. Rev. Comput. Stat.* **3**, 180–185 (2011).

Acknowledgements

This research was funded by the RETURN Extended Partnership funded by the European Union Next-Generation EU (National Recovery and Resilience Plan–NRRP, Mission 4, Component 2, Investment 1.3–D.D. 1243 2/8/2022, PE0000005), by the National Biodiversity Future Center (National Recovery and Resilience Plan–NRRP, Mission 4, Component 2, Investment 1.4, CN00000033). This work was supported by funding from the European Research Council (ERC) under the European Union's Horizon 2020 research and innovation program Grant Agreement No. 948972—COEVOLVE—ERC-2020-STG. The authors wish to thank Guglielmo Fragale, Claudio Cipriani and the staff of the diving center Centro Sub Pozzuoli for assistance with the boat and diving operations. The authors gratefully acknowledge Francesco Guerra for granting permission to use the photographs included in this publication. Finally, we extend our sincere thanks to Ana Clara Pelliciari Silva, Jacopo Brusca, Isabel Bassolino, Francesco Montemagno, Martina Cascone, and Deborah Bastoni from the Department of Biology (University of Naples Federico II) for their valuable assistance and support during the sampling campaigns.

878

879 Author contributions

880 A.S.V., F.M., S.C.D., S.C., M.A.D.V., D.G., and A.A., drafted the original version of the manuscript.
881 A.A., D.G., S.C. and M.M conceived the study design. A.S.V., F.M., S.C.D and S.C. contributed to
882 geochemical and microbiological data collection and analysis. GS generated the ocean circulation
883 model. All coauthors contributed to editing the final version of the manuscript.

884 Competing interests

885 The authors declare no competing interests.

Figures

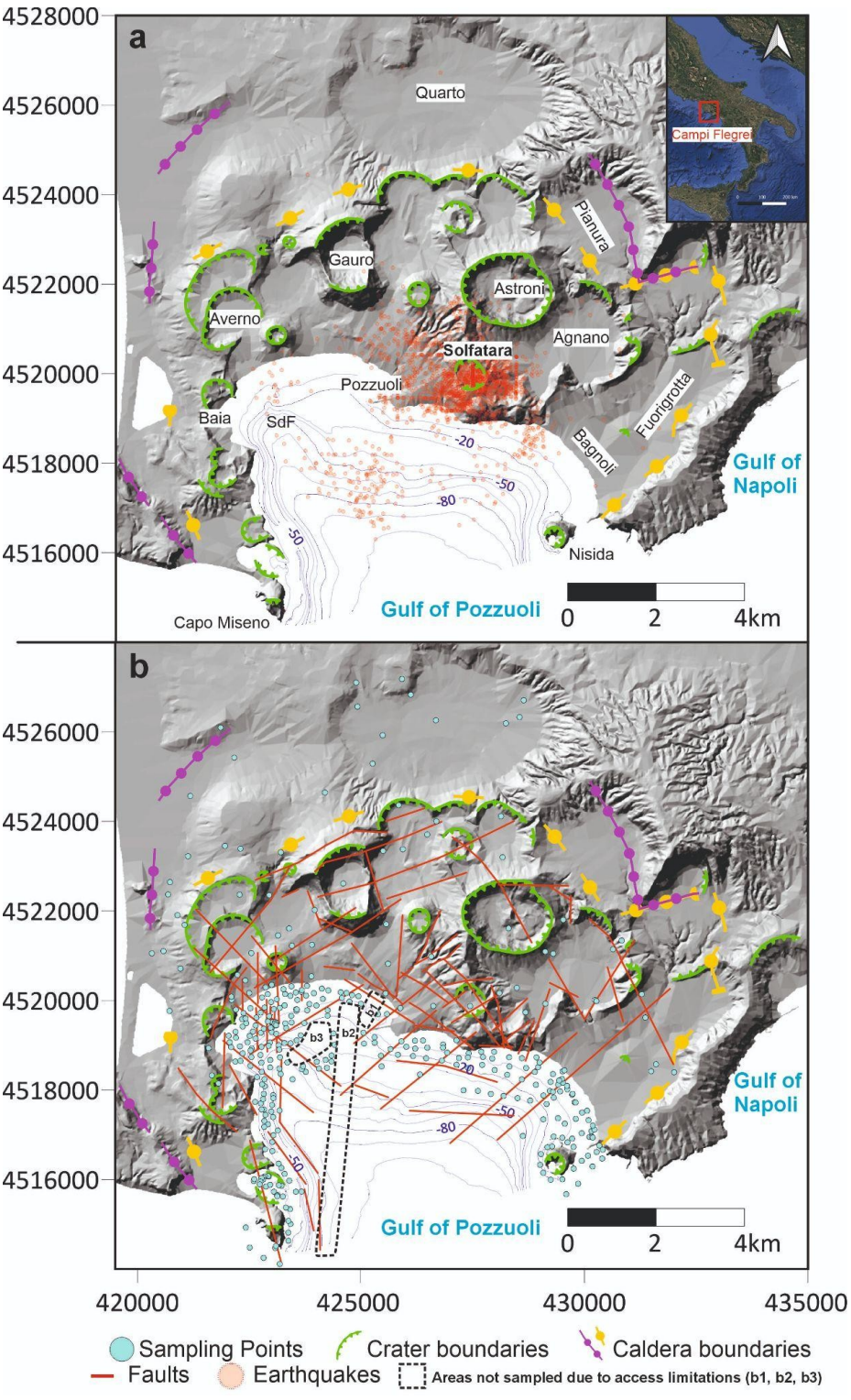

Figure 1. Map of Campi Flegrei caldera (CFc). These maps show the main localities, main geological structures[36,67,73], seismicity after 2022[27], bathymetry (given in meters) and sampling points. Areas not sampled due to access limitations are: b1) Pozzuoli harbour, b2) high-traffic navigation corridor and b3) the mytilid aquaculture facility. SdF: Secca delle Fumose. The image at the top right of panel a was taken from Google Earth Pro version 7.3.6.10441.

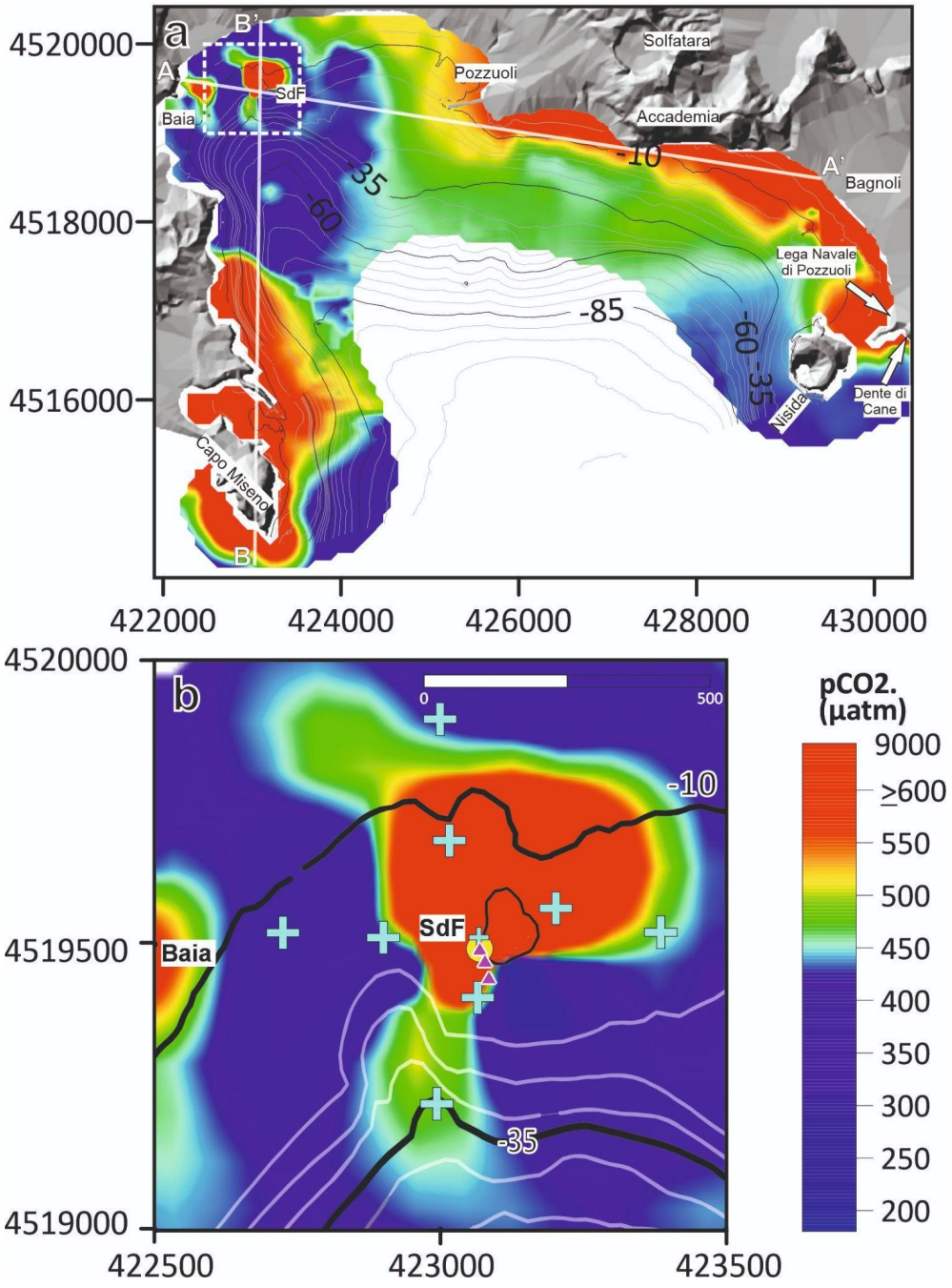

Figure 2. Distribution of pCO_2 at the base of the seawater column along the Pozzuoli Bay. a) The map was generated using the maximum pCO_2 value (pCO_2 max) measured at the deepest point of each station (see Supplementary Tables 1 and 2). Major anomalies were found in SdF (up to 9000 µatm), Accademia-Bagnoli-Nisida coast (up to 4420 µatm), Baia Castle beach (up to 850 µatm) and Capo Miseno (up to 2300 µatm). Black and gray solid lines represent bathymetry which is given in meters. Solid white lines represent the profiles A-A'and B-B' of Fig. 3. The white square represents the location of panel b, which is a closer view of the SdF anomaly. In this area, pCO_2 probing was coupled with the collection of biological samples, including biofilms (violet triangle), vent fluids (yellow circle), and seawater (blue cross). Samples from seawater column were collected along two transects, one N-S (sites T1, T2, T4, T5) and one W-E (sites T6, T7, T8, T9) centered on (site T3).

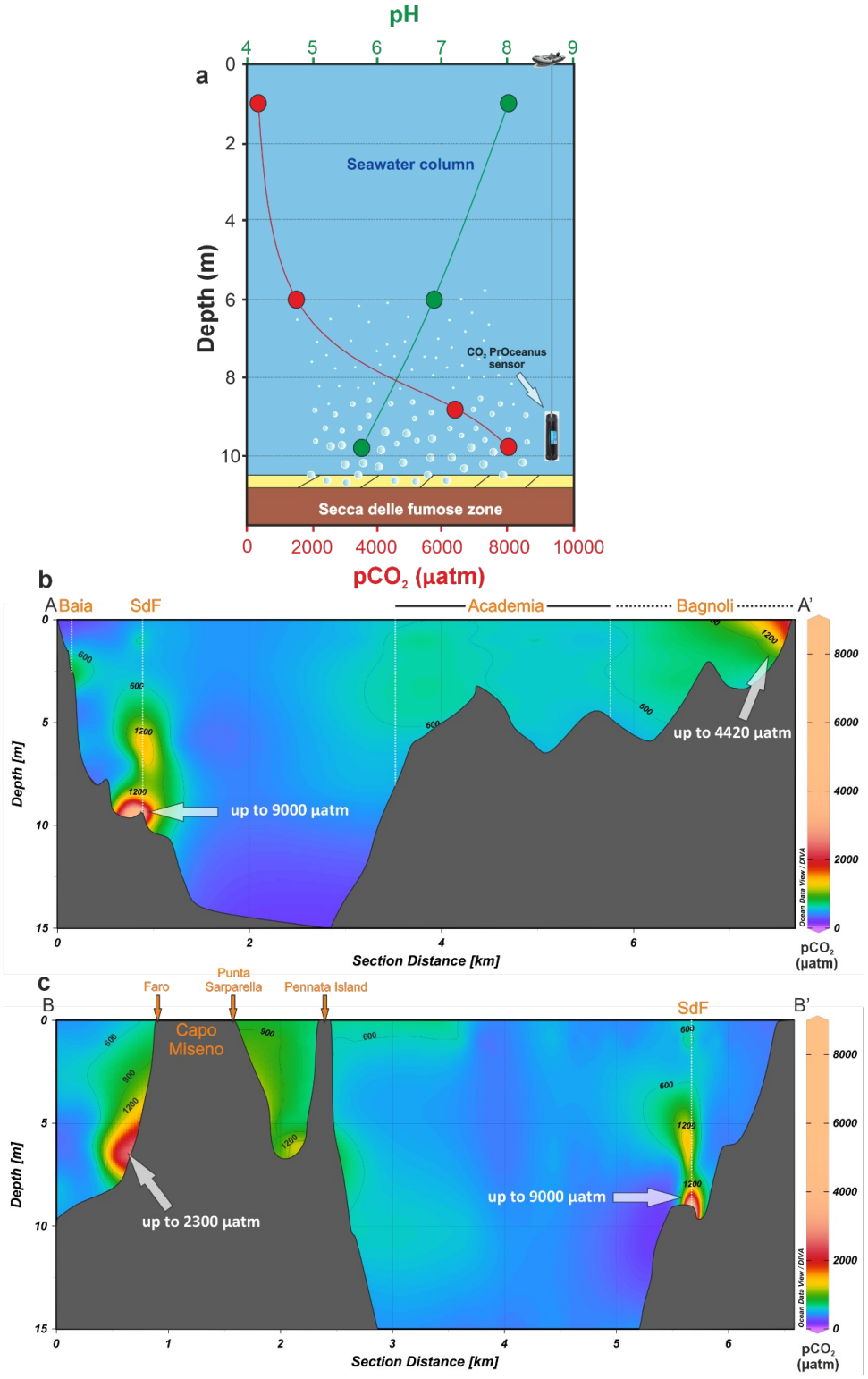

Figure 3. Vertical variability of pCO_2 and pH in seawater above the SdF zone. a) A profile showing the change of pCO_2 and pH directly above the SdF geyser using data presented in Supplementary Table 2. b-c) Profiles showing the variability of pCO_2 in the seawater column and the distribution of the main hydrothermal hotspots along the Pozzuoli Gulf. Profiles AA' and BB' can be also observed in the map of Fig. 2. Data interpolation was achieved using DIVA Gridding available in ODV software (further details are presented in the "Methods" section).

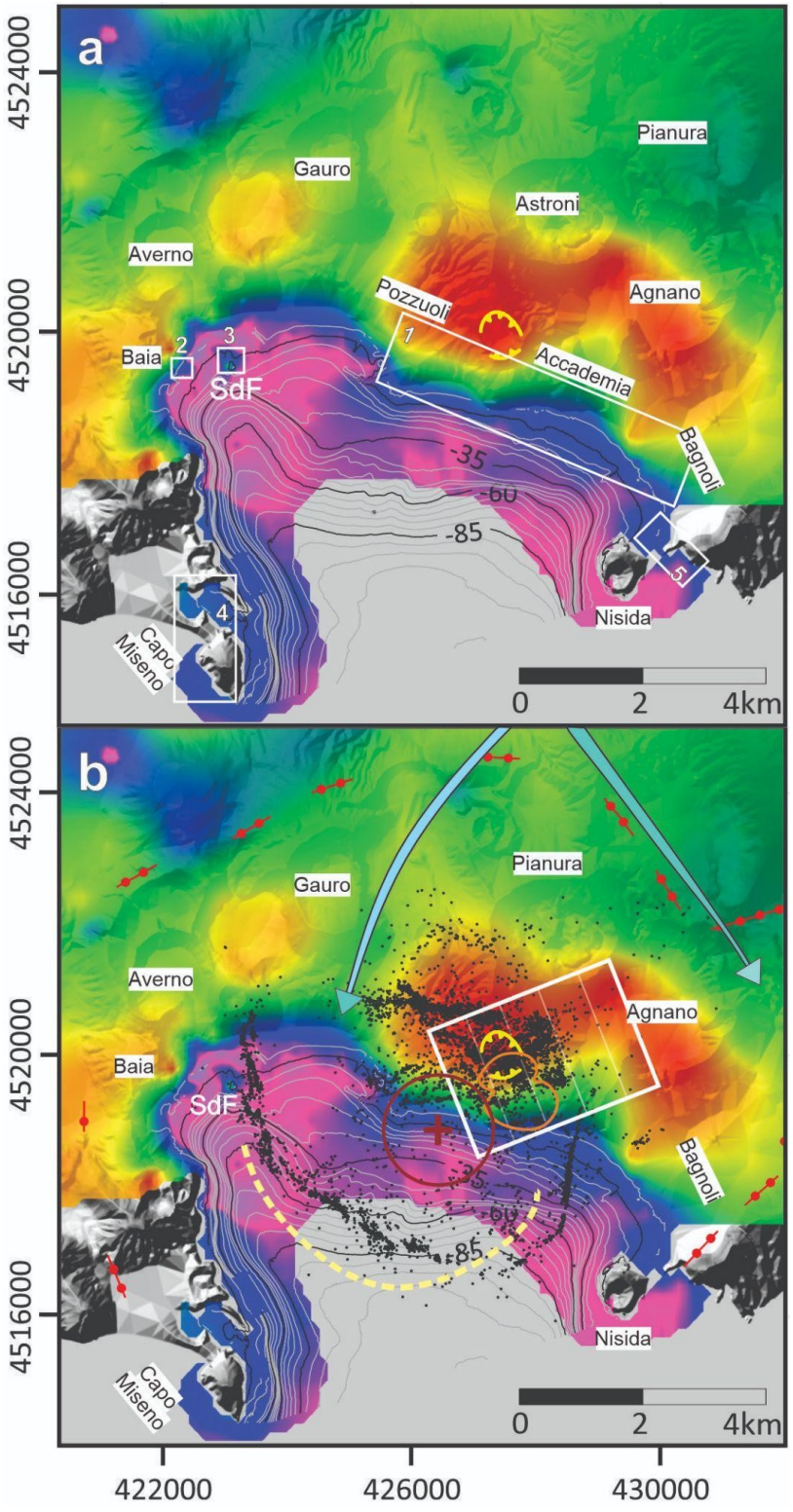

Figure 4. Maps of CFc showing the pCO_2 distribution in seawater (Pozzuoli Bay) and groundwater. a) Regarding the Pozzuoli Bay, the map was generated using the maximum pCO_2 value (pCO_2 max) measured at the deepest point of each station. White squares indicate the main sectors (1 to 5) where pCO_2 is anonymously high in seawater. b) Map of CFc comparing the pCO_2 distribution in water and the main morpho-structural elements observed in the caldera: The red lines (with red circles) represent the outer caldera rim bordering faults and the solid yellow lines the boundary of the Solfatara

crater[67,25]; the white square and the white lines indicate the orientation (N 249° ± 4°, 53° ± 1°) of the potential incipient volcanotectonic fault (PIF)[70]. The dotted pale yellow line represents the base of the resurgent dome while the red circle (and cross in the center) shows the area with the maximum resurgence[39]; the orange polygon represents the Accademia geodetic anomaly[71]; the black dots indicates the seismicity after 2022[27] while the blue long arrows show the aquifer main preferential drainage in the Campi Flefrei area[32]. Both maps were generated using the data of Supplementary Tables 1 and 2).

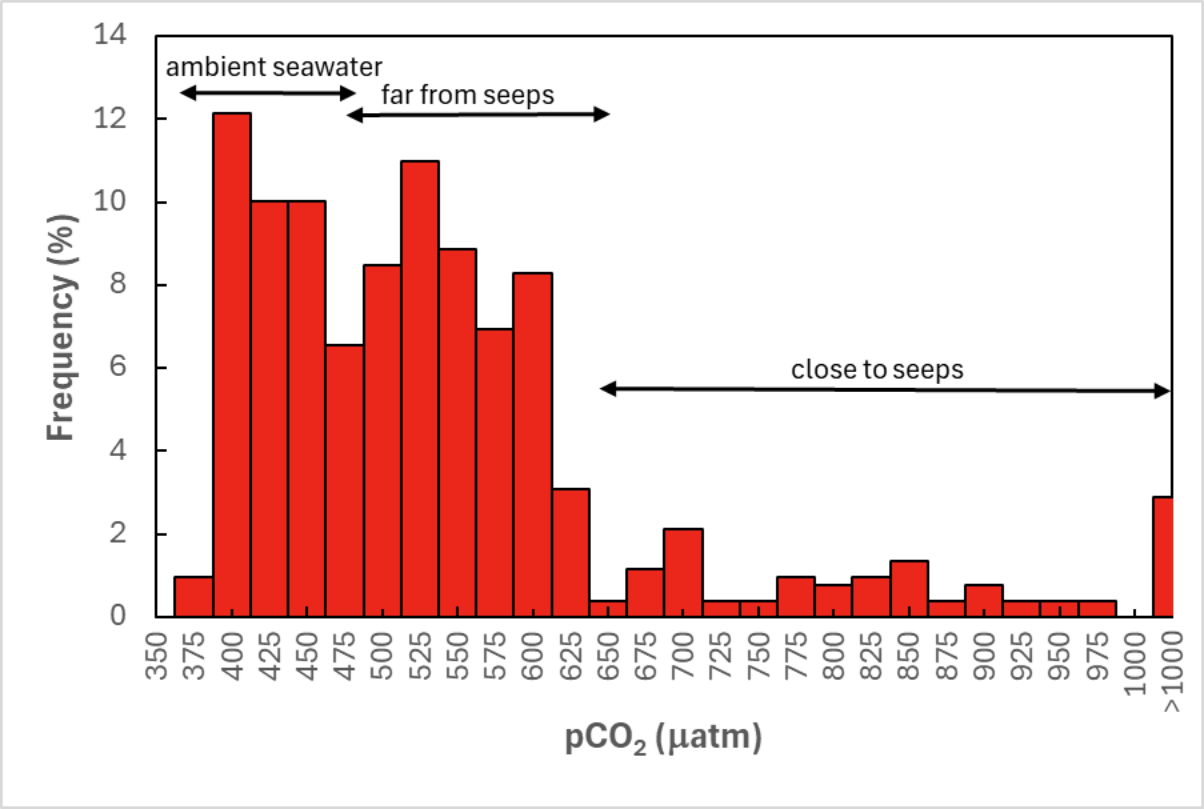

Figure 5. **Frequency distribution diagram of seawater pCO_2 values in the CFc offshore.** Data are interpreted as a mixture of 3 distinct populations.

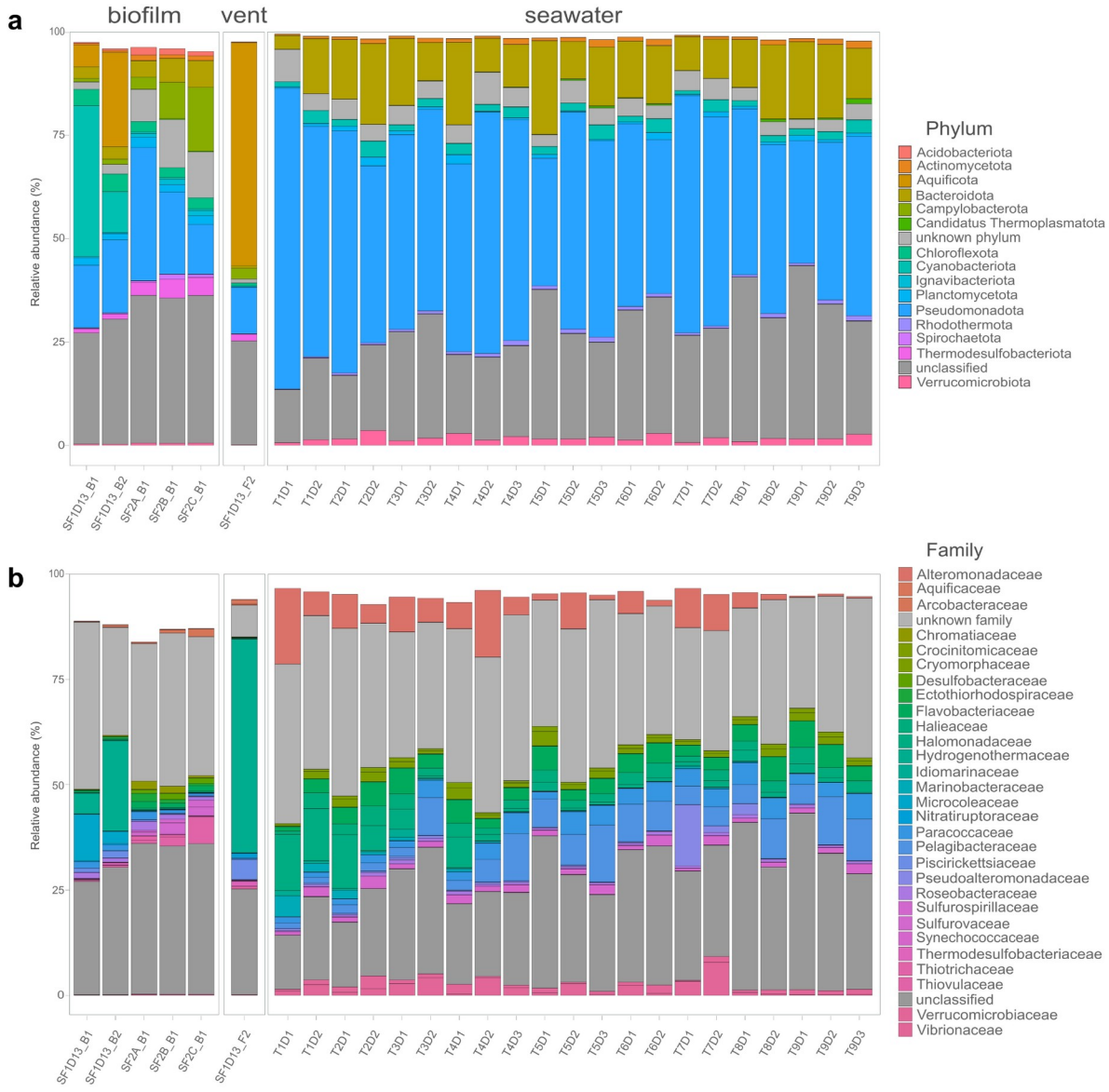

936

937 **Figure 6**. **Microbial community composition across the SdF hydrothermal system.** (a) Relative
938 taxonomic composition at the phylum level and (b) at the family level across biofilms, hydrothermal
939 vent fluids, and seawater samples. Samples are grouped by environmental compartment, highlighting
940 compositional contrasts between vent-associated communities and the surrounding seawater.

941

942

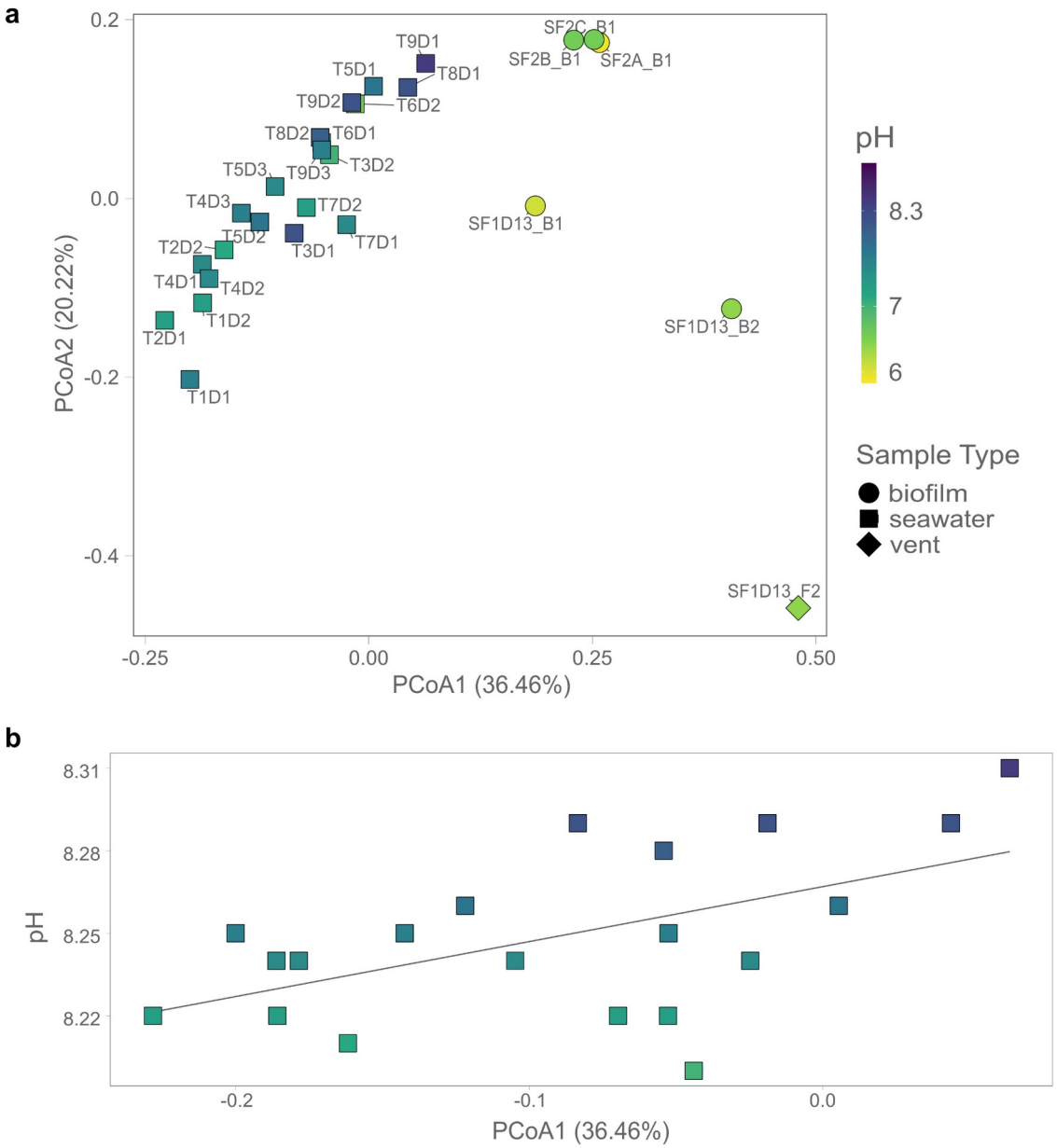

943

944 **Figure 7. Beta diversity patterns of microbial communities in the SdF area.** (a) Principal
945 Coordinates Analysis (PCoA) based on weighted Jaccard dissimilarity at the genus level. Symbols are
946 shaped by sample type (biofilms, circles; seawater, squares; vent fluids, diamonds) and colored by pH.
947 (b) Relationship between PCoA axis 1 and pH for seawater samples (Pearson correlation, $r^2 = 0.549$, p
948 = 0.012; n=20).

949

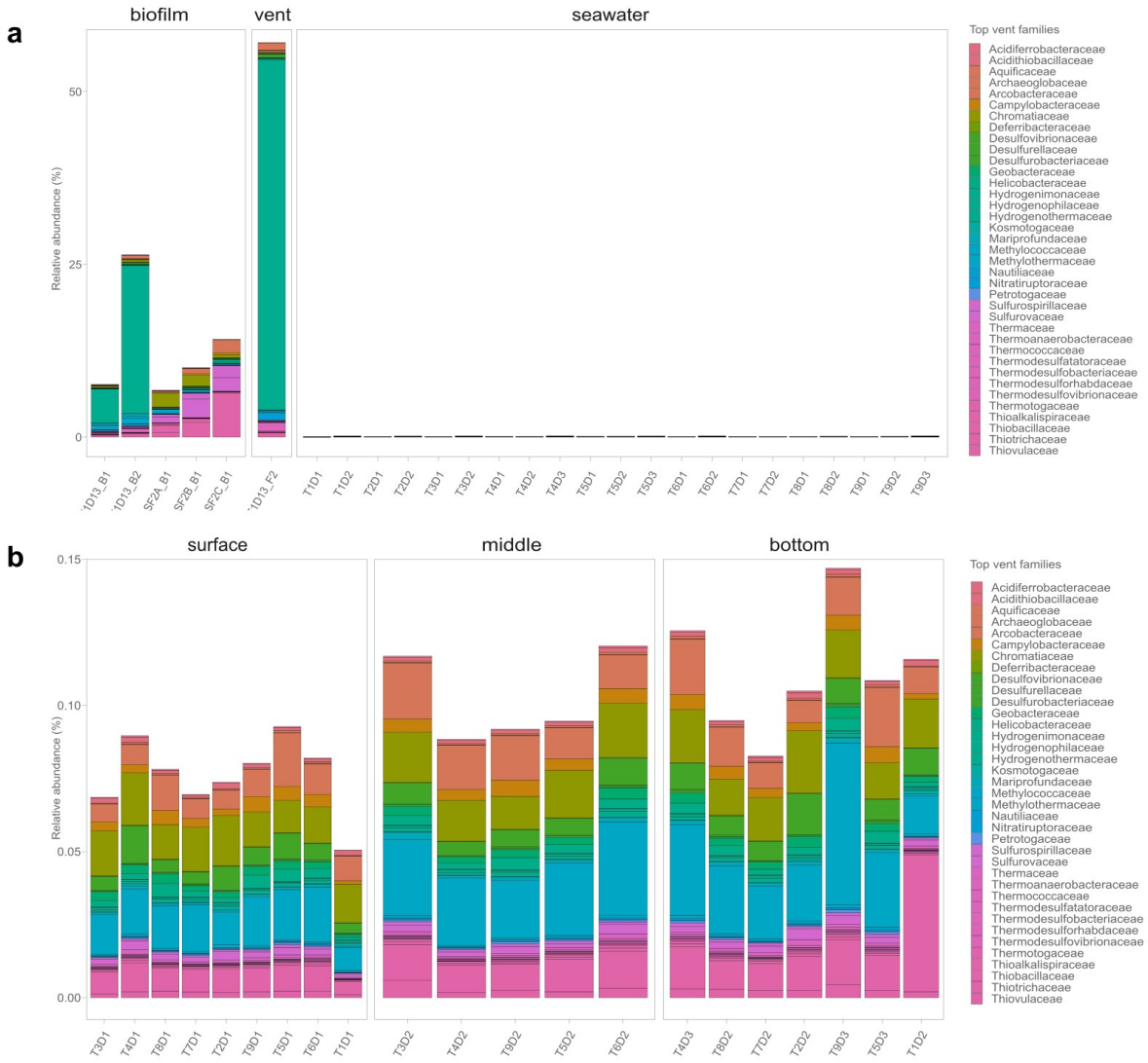

950

951 **Figure 8. Distribution of vent-associated microbial families in the SdF area.** (a) Relative abundance
952 of selected vent-associated families across biofilm, hydrothermal vent fluid, and seawater samples. (b)
953 Seawater samples shown by depth layer (surface, middle, bottom) and ordered by increasing distance
954 from the SdF vent within each depth, highlighting dilution patterns away from the source.

955

956

957

958

959

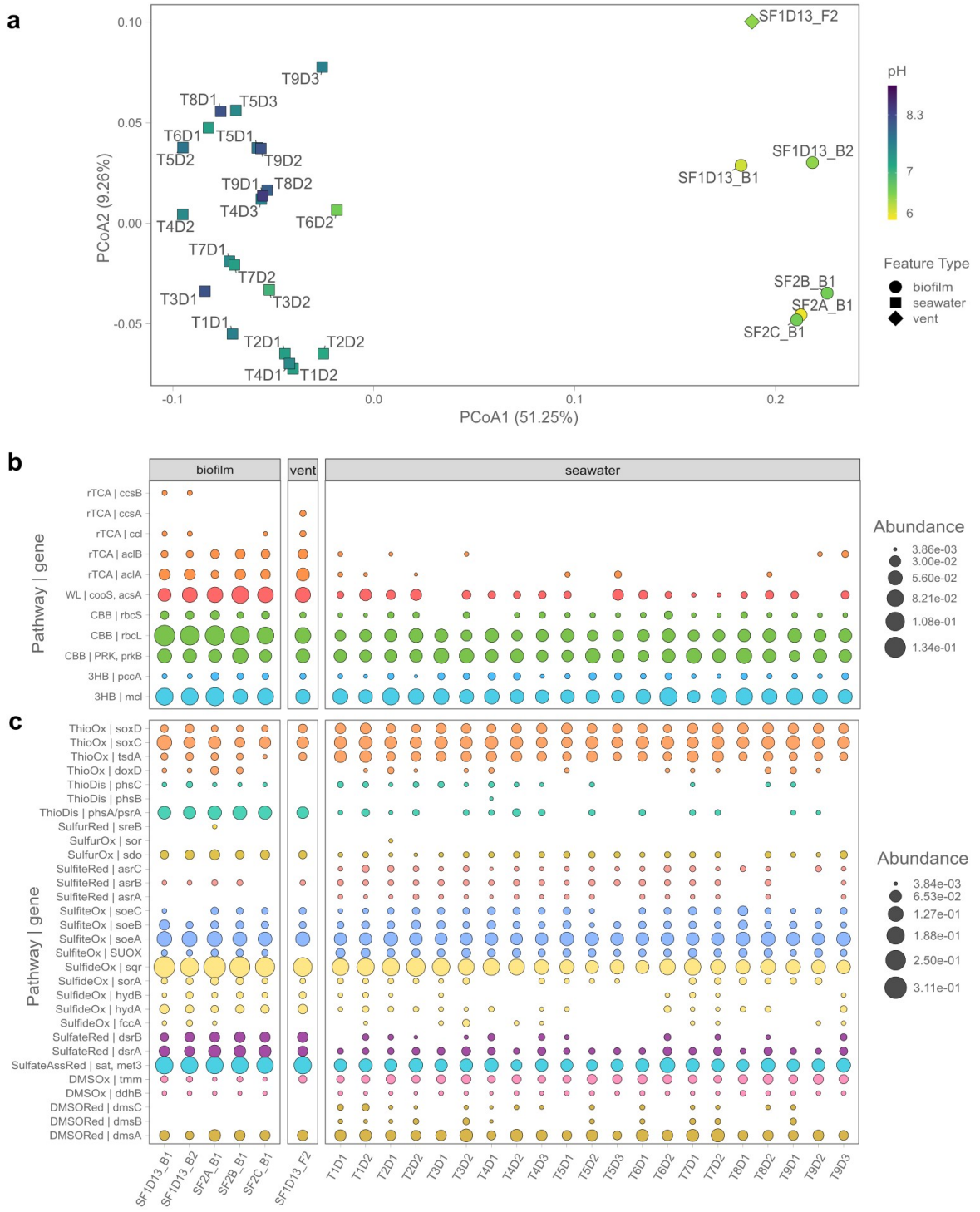

960

961 **Figure 9. Functional potential of microbial communities across the SdF hydrothermal system.** (a)
962 Principal Coordinates Analysis (PCoA) based on weighted Jaccard dissimilarity of functional gene
963 profiles. Symbols are shaped by sample type (biofilms, circles; seawater, squares; vent fluids,
964 diamonds) and colored by pH. (b) Bubble plot showing the relative abundance of key genes involved
965 in carbon fixation pathways (rTCA, reductive tricarboxylic acid cycle; WL, Wood–Ljungdahl pathway;
966 CBB, Calvin–Benson–Bassham cycle; 3HB, 3-hydroxypropionate bicycle) across samples. (c) Bubble

967 plot showing the relative abundance of key genes involved in sulfur metabolism (thiosulfate oxidation
968 and disproportionation; sulfur, sulfite, sulfide, and sulfate oxidation and reduction; and dimethyl sulfide
969 oxidation and reduction). In panels B and C, bubble size is proportional to gene relative abundance.

Supplementary Materials

Supplementary Figures

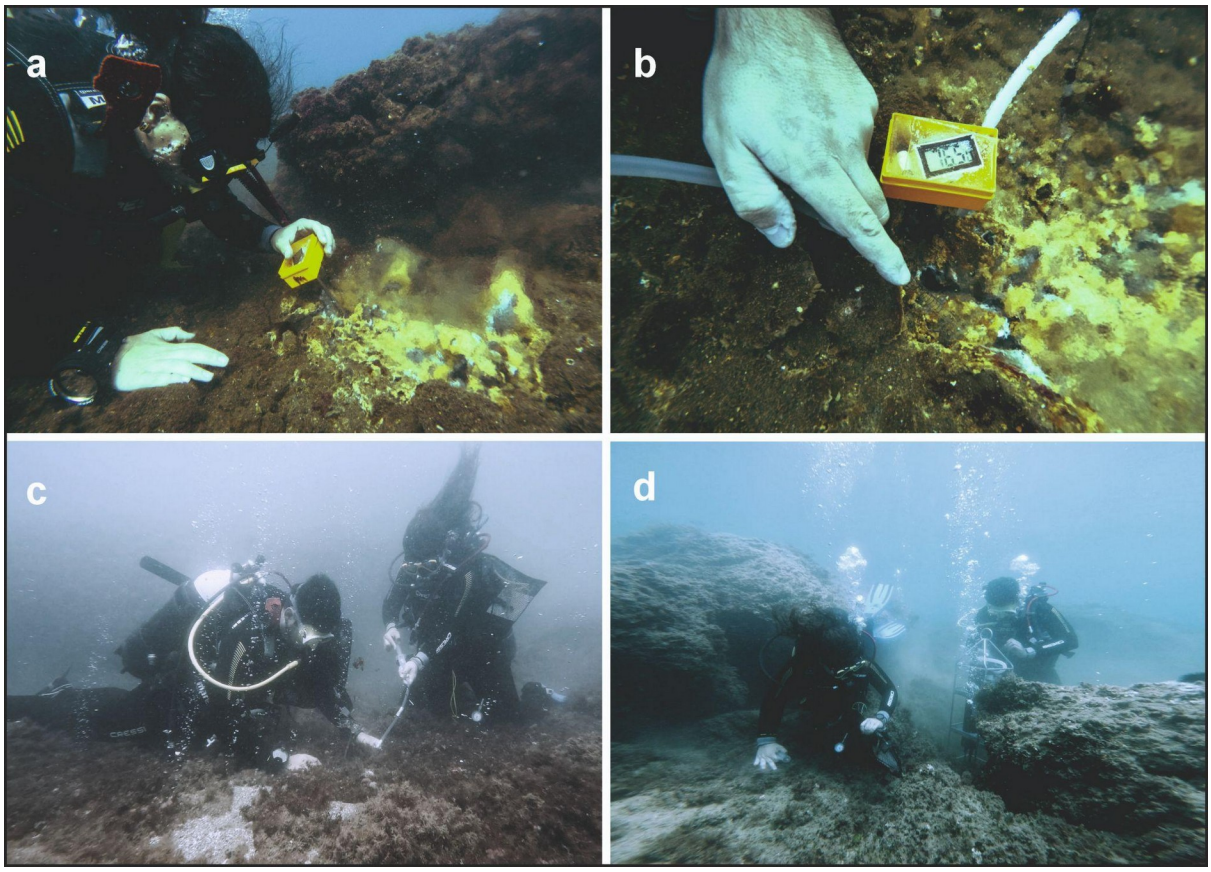

Supplementary Figure 1. Geochemical and microbiological sampling at Pozzuoli bay. SdF area (a, b) and Capo Miseno (c, d) near El Faro (see Fig. 3c). Photos by Francesco Guerra used with permission.

978

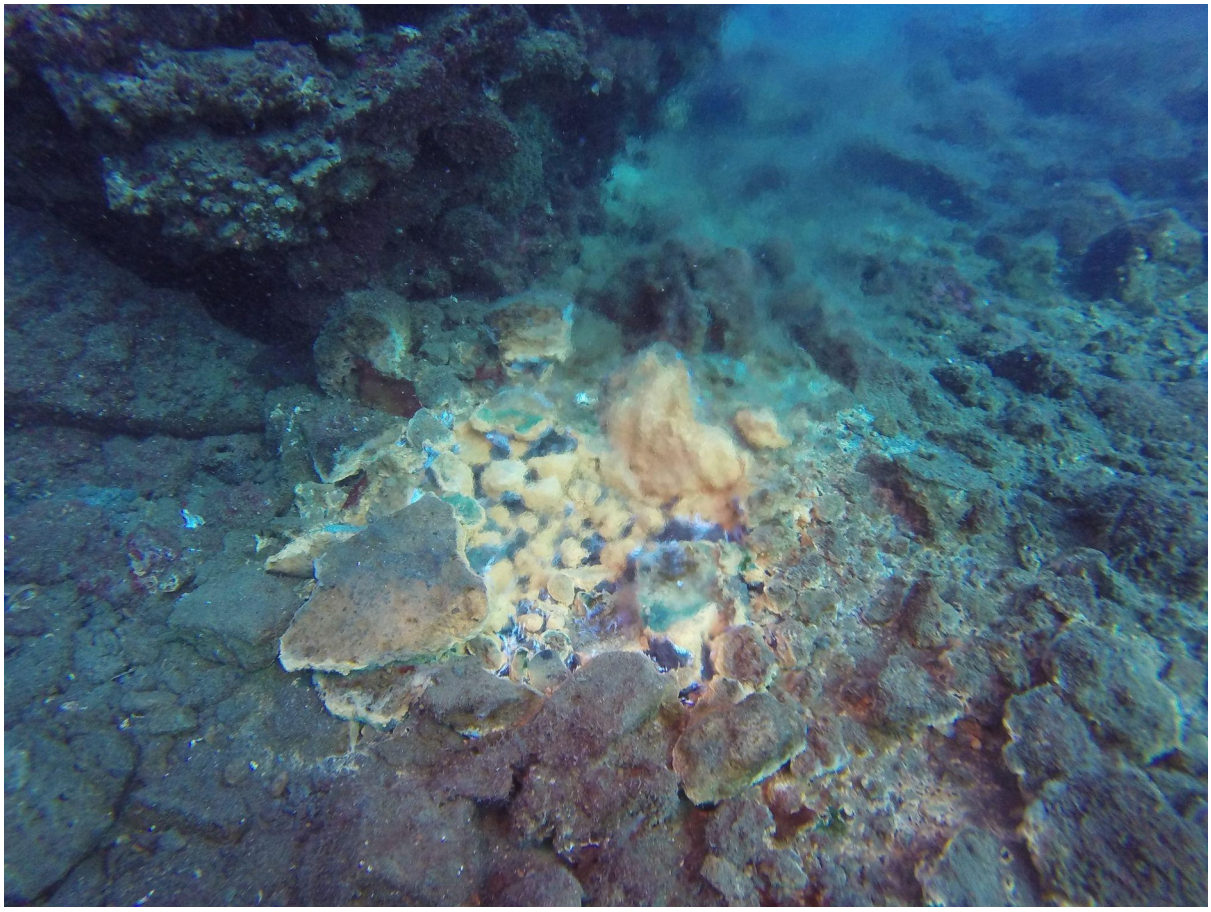

979

980 **Supplementary Figure 2. A close up view of the Secca delle Fumose main emission site**
981 **(SF1D13)**. The orange and green biofilm are visible.

982

983

984

985

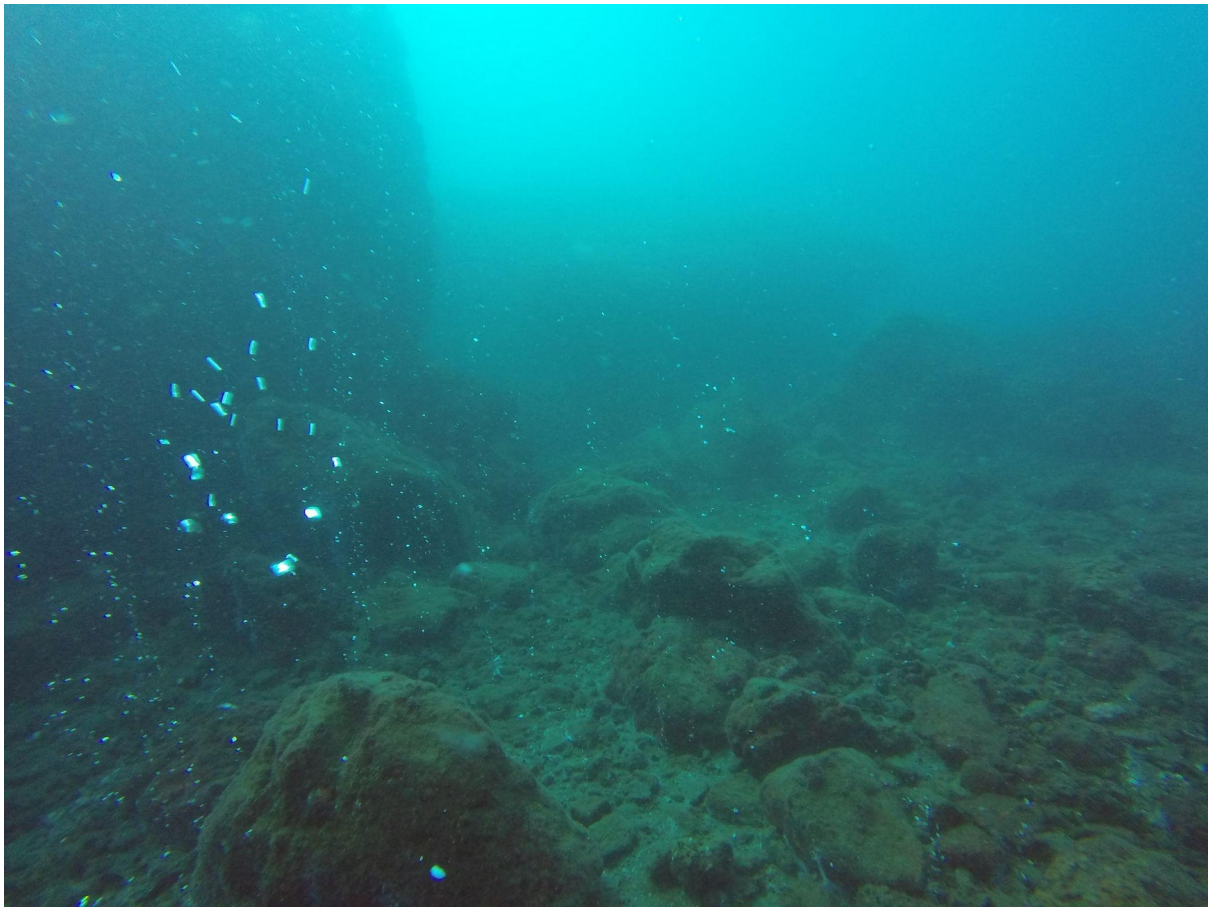

Supplementary Figure 3. Area of lower temperature degassing near Secca delle Fumose.

991

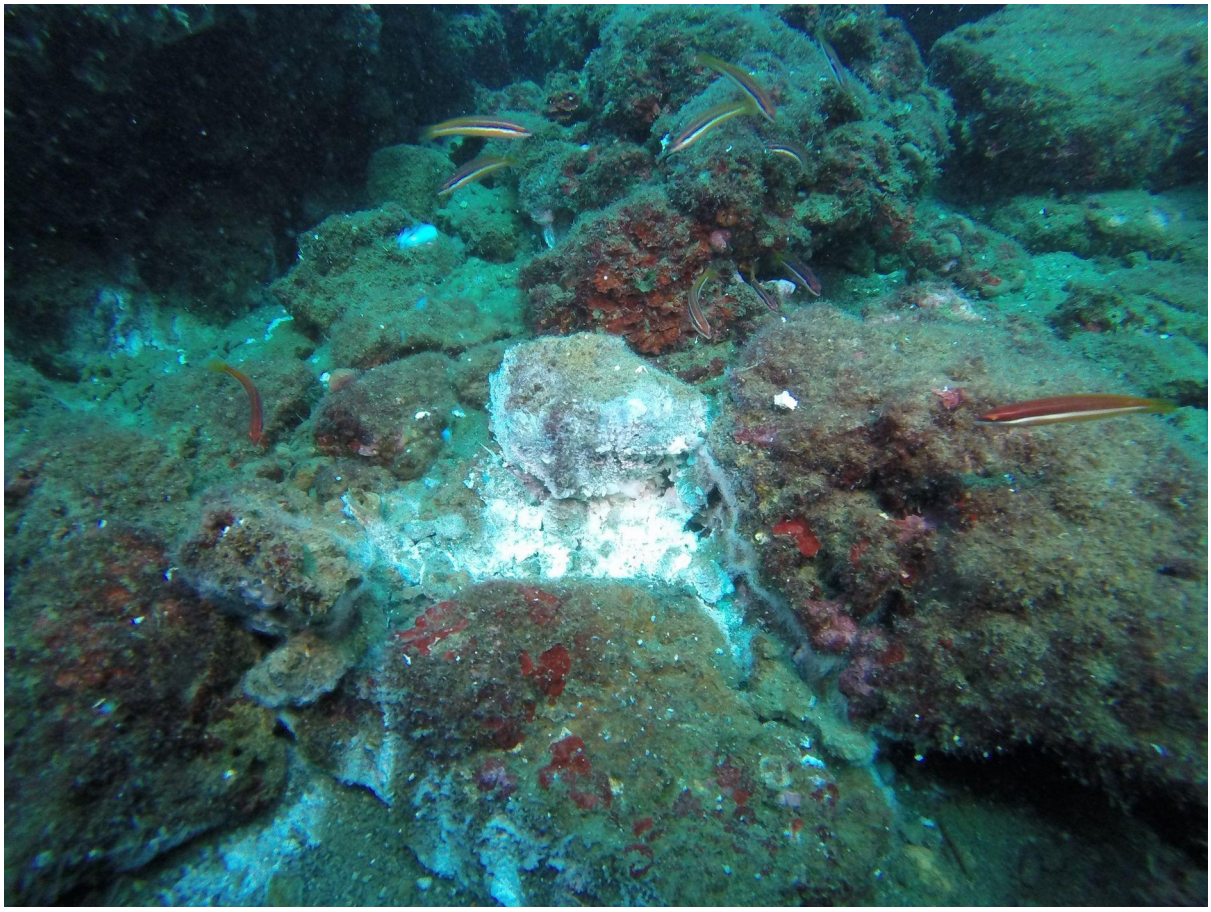

992

993 **Supplementary Figure 4. Area of low temperature emission at Secca delle Fumose**. Low
994 temperature white biofilms (SF2 samples) in the

995

996

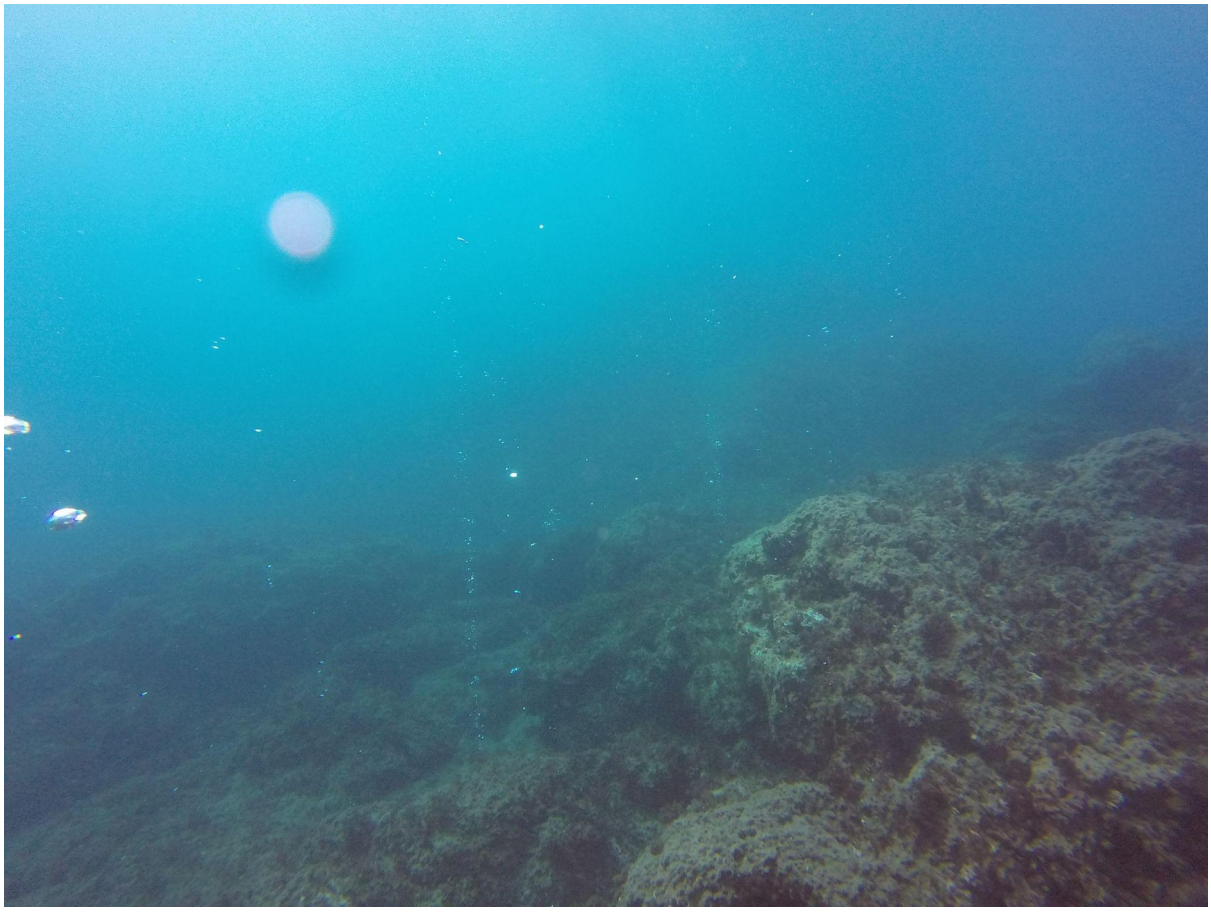

Supplementary Figure 5. Presence of visible degassing in the area of Capo Miseno.

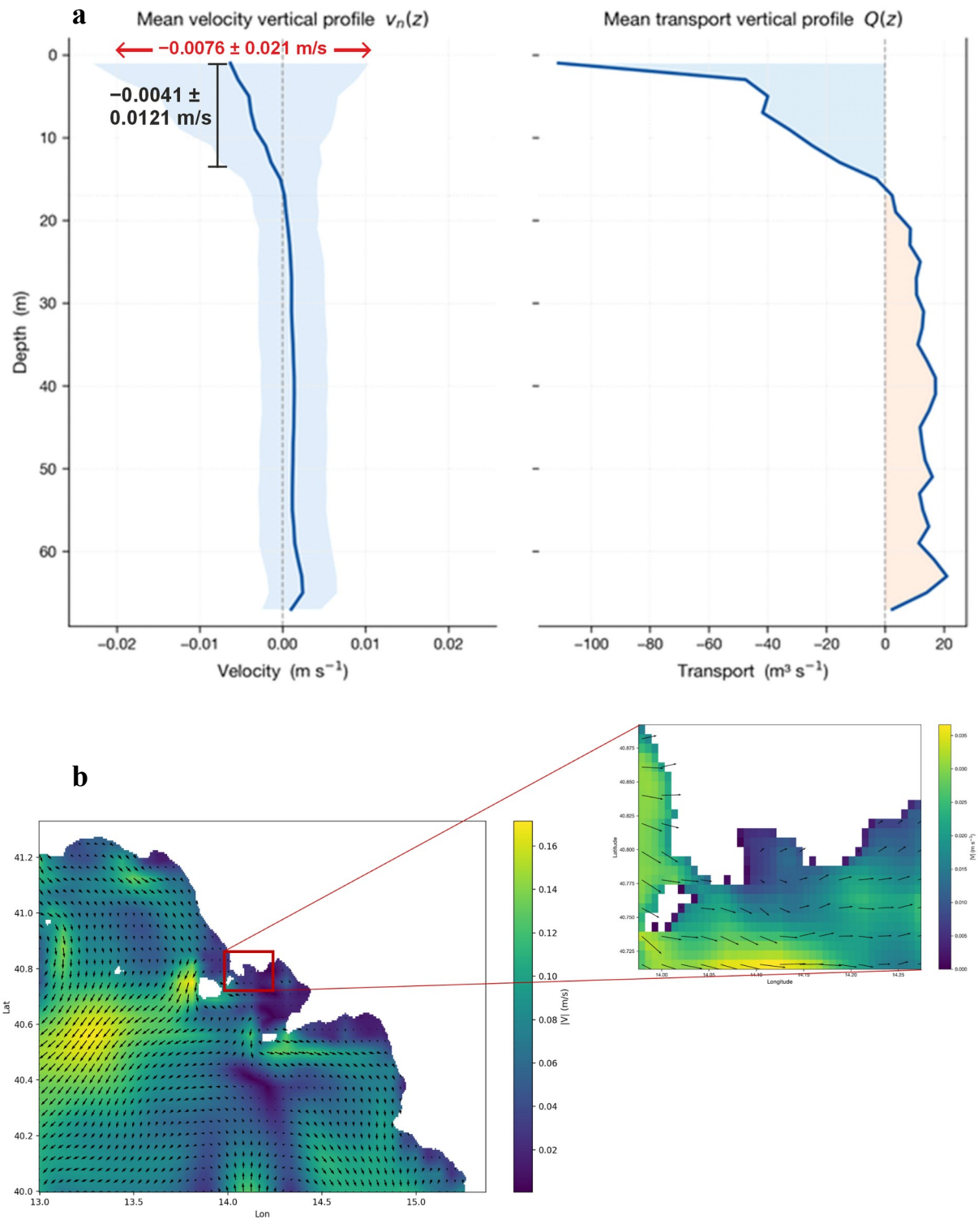

Supplementary Figure 6: Vertical profile of annual mean velocity (in m/s) and transport (in m3/s) across the Baia–Bagnoli transect. a) Positive values indicate flow out of the gulf normal to the section, whereas negative values indicate flow into the gulf. Values were converted from sigma coordinates to physical depths and averaged along the section using area-weighted binning. Shading in the left panel

represents the standard deviation of the annual mean velocity. Shadings in the right panel represents the net landward (blue) and seaward (red) transport. Statistics were computed after excluding the spin-up period. b) Surface velocity field showing the study area and a zoomed-in view of the Gulf of Pozzuoli. Colors represent current speed and arrows indicate flow direction.

Supplementary Table 1. pCO_2 values obtained from Seawater Vertical Profiles in the Pozzuoli Bay and from given in meters below sea level (b.s.l). Excess of carbon for each seawater point was calculated in reference to

Station	East X	North Y	Bottom Depth [m]	Depth [m]	pCO2 Max (µatm)	pCO2 (error +/-)
BG	423146	4518995.7	18	2	498	2.5
BG	423146	4518995.7	18	7	477	2.4
BG	423146	4518995.7	18	15	446	2.2
29	423089	4519440.4	15	2	513	2.6
29	423089	4519440.4	15	7	512	2.6
29	423089	4519440.4	15	13	518	2.6
SF1	423069	4519492.4	10	2	514	2.6
SF1	423069	4519492.4	10	7	1428	7.1
39	423095	4519503.3	11	2	522	2.6
45	422993	4519388.9	15	3	575	2.9
45	422993	4519388.9	15	8	529	2.6
46	422990	4519285.6	15	3	529	2.6
46	424158	4630303.2	15	7	523	2.6
46	425350	4741339.6	15	13	528	2.6
47	423006	4519514.2	11	2	534	2.7
47	423006	4519514.2	11	6	533	2.7
47	423006	4519514.2	11	10	532	2.7
48	423105	4519594.2	8	2	577	2.9
48	423105	4519594.2	8	7	532	2.7
54	422180	4519297.5	4	3	460	2.3
56	422494	4519203.1	10	1	423	2.1
56	422494	4519203.1	10	9	477	2.4
58	422626	4519144	14.3	6	425	2.1
58	422626	4519144	14.3	12	434	2.2
62	422569	4519301.1	10	5	422	2.1
62	422569	4519301.1	10	9	421	2.1
66	422327	4519579	3	3	849	4.2
70	422418	4519488.1	7	1	452	2.3
70	422418	4519488.1	7	6	549	2.7
72	422629	4519438.2	10	5	452	2.3
76	422904	4519527.9	12	1	438	2.2
86	422742	4519725.6	7	1	480	2.4
88	422934	4519645.9	11	1	470	2.4
88	422934	4519645.9	11	5	506	2.5
88	422934	4519645.9	11	10	487	2.4
90	423036	4519802.5	9.3	1	518	2.6
90	423036	4519802.5	9.3	8	518	2.6
92	422827	4519838	6	5	536	2.7
96	422772	4520062.8	2	1	422	2.1
112	422047	4519388.8	3	2	470	2.4
119	422024	4519207	5	3	476	2.4
121	422187	4519147.5	5.6	3	437	2.2

142	422047	4519062.4	4	2	423	2.1
144	422078	4518898.9	5	3	436	2.2
154	422173	4518631.4	2	1	435	2.2
155	422290	4518643.5	8	1	433	2.2
156	422539	4518545.4	25	1	427	2.1
162	422660	4518281	5	2	427	2.1
164	422800	4518144.1	25	1	428	2.1
179	422616	4517730.8	6	3	431	2.2
184	423289	4520138.5	2	1	443	2.2
185	423251	4520248.8	3.6	2	450	2.3
186	423406	4520099.5	5.18	3	442	2.2
187	423430	4520312.4	2	1	457	2.3
188	423527	4520174.9	3.6	2	475	2.4
189	423562	4520008	5.2	3	445	2.2
190	423783	4519777	10	1	439	2.2
190	423783	4519777	10	4	445	2.2
190	423783	4519777	10	9	448	2.2
191	423831	4519915.3	6.6	3	468	2.3
192	423757	4520104.8	2	1	478	2.4
193	423654	4520190.2	2	1	483	2.4
194	423665	4520226.7	3	1	480	2.4
195	423426	4519651.9	10	1	460	2.3
195	423426	4519651.9	10	4	453	2.3
195	423426	4519651.9	10	9	451	2.3
196	423145	4519027.6	43	1	454	2.3
196	423145	4519027.6	43	7	438	2.2
198	423055	4518877.5	-	1	453	2.3
198	423055	4518877.5	-	7	436	2.2
200	423123	4518712.5	54.2	1	449	2.2
200	423123	4518712.5	54.2	7	427	2.1
202	423144	4518589	48.3	1	452	2.3
202	423144	4518589	48.3	7	426	2.1
204	423268	4518252.5	64	1	486	2.4
204	423268	4518252.5	64	7	435	2.2
204	423268	4518252.5	64	15	442	2.2
206	423455	4518232.8	60.9	1	475	2.4
206	423455	4518232.8	60.9	7	434	2.2
208	423387	4518529.9	60	1	480	2.4
208	423387	4518529.9	60	7	449	2.2
210	423398	4518548.7	59.9	1	480	2.4
210	423398	4518548.7	59.9	7	451	2.3
212	423433	4519503.1	14	1	502	2.5
212	423433	4519503.1	14	6	469	2.3
212	423433	4519503.1	14	13	423	2.1
213	423091	4519252.4	20	1	490	2.5
213	423091	4519252.4	20	7	456	2.3
213	423091	4519252.4	20	15	432	2.2

214	423078	4519437.9	9	1	473	2.4
214	423078	4519437.9	9	4	466	2.3
214	423078	4519437.9	9	8	428	2.1
216	422964	4519385.8	15	7	491	2.5
216	422964	4519385.8	15	14	519	2.6
217	423292	4519484.6	12	1	488	2.4
217	423292	4519484.6	12	5	462	2.3
217	423292	4519484.6	12	11	443	2.2
218	423312	4519377.8	15.3	1	487	2.4
218	423312	4519377.8	15.3	7	464	2.3
218	423312	4519377.8	15.3	14	429	2.1
219	423413	4519305.7	-	1	489	2.4
220	423552	4519796.1	8	1	500	2.5
220	423552	4519796.1	8	6	468	2.3
221	423931	4520157.4	3	1	491	2.5
222	423777	4520321.1	2.7	1	527	2.6
223	424109	4520259.9	3	1	479	2.4
224	424132	4520029.9	6	3	486	2.4
225	423189	4518355.4	61	1	507	2.5
225	423189	4518355.4	61	7	460	2.3
227	424046	4518474.3	45	1	498	2.5
227	424046	4518474.3	45	7	445	2.2
229	424224	4518490.2	38	1	496	2.5
229	424224	4518490.2	38	7	444	2.2
231	424327	4518632.4	29	1	496	2.5
231	424327	4518632.4	29	7	451	2.3
233	424394	4519005.8	27	1	487	2.4
233	424394	4519005.8	27	7	457	2.3
233	424394	4519005.8	27	15	426	2.1
236	424239	4519777.9	16	1	512	2.6
236	424239	4519777.9	16	7	436	2.2
237	424238	4519656.9	18	1	509	2.5
237	424238	4519656.9	18	7	481	2.4
237	424238	4519656.9	18	15	439	2.2
238	424255	4520219.6	3	1	505	2.5
241	425892	4519083.9	6	1	695	3.5
241	425892	4519083.9	6	5	620	3.1
242	426195	4519096	5	3	644	3.2
243	426543	4519099.6	3.2	1	657	3.3
244	426823	4519011.9	5	3	576	2.9
245	427100	4518938.7	6	1	675	3.4
245	427100	4518938.7	6	5	585	2.9
246	427398	4518815.4	7.2	1	617	3.1
246	427398	4518815.4	7.2	6	582	2.9
247	427677	4518849.4	5	3	599	3.0
248	427965	4518848.2	5.2	3	591	3.0
249	428302	4518727.7	6	1	687	3.4

249	428302	4518727.7	6	5	602	3.0
250	428587	4518706.5	5	3	708	3.5
251	428913	4518724.4	2	1	732	3.7
252	428874	4518397.7	7.6	1	670	3.4
252	428874	4518397.7	7.6	5	560	2.8
253	428585	4518232.7	13	1	598	3.0
253	428585	4518232.7	13	6	577	2.9
253	428585	4518232.7	13	12	560	2.8
254	428258	4518333.8	15	1	550	2.8
254	428258	4518333.8	15	6	538	2.7
254	428258	4518333.8	15	12	522	2.6
255	427978	4518442.3	13	1	542	2.7
255	427978	4518442.3	13	6	539	2.7
255	427978	4518442.3	13	12	513	2.6
256	427698	4518556.6	11	1	539	2.7
256	427698	4518556.6	11	5	541	2.7
256	427698	4518556.6	11	9	539	2.7
257	427383	4518486.7	18	1	575	2.9
257	427383	4518486.7	18	7	536	2.7
257	427383	4518486.7	18	15	482	2.4
258	427125	4518560.9	19	1	606	3.0
258	427125	4518560.9	19	7	514	2.6
258	427125	4518560.9	19	15	498	2.5
259	426799	4518654.3	18	1	609	3.0
259	426799	4518654.3	18	7	510	2.6
259	426799	4518654.3	18	15	471	2.4
260	425176	4518717.4	20	1	614	3.1
260	425176	4518717.4	20	7	500	2.5
260	425176	4518717.4	20	15	479	2.4
261	426151	4518755.2	18	1	590	3.0
261	426151	4518755.2	18	7	505	2.5
261	426151	4518755.2	18	15	521	2.6
262	423085	4519442.6	10	10	695	3.5
263	423069	4519455.9	10	9	1188	5.9
264	423078	4519487.9	10.8	8	818	4.1
265	423054	4519467.4	9.3	1	693	3.5
269	425812	4518783.7	18	1	553	2.8
269	425812	4518783.7	18	7	549	2.7
269	425812	4518783.7	18	15	526	2.6
270	425433	4518761.6	25	1	548	2.7
270	425433	4518761.6	25	7	574	2.9
270	425433	4518761.6	25	15	520	2.6
271	428772	4517757.8	25	1	585	2.9
271	428772	4517757.8	25	7	555	2.8
271	428772	4517757.8	25	15	513	2.6
272	428491	4517813.1	28	1	553	2.8
272	428491	4517813.1	28	7	506	2.5

272	428491	4517813.1	28	15	489	2.4
273	428177	4517862.9	31	1	548	2.7
273	428177	4517862.9	31	7	533	2.7
273	428177	4517862.9	31	15	470	2.4
274	427892	4517908.6	33	1	549	2.7
274	427892	4517908.6	33	7	520	2.6
274	427892	4517908.6	33	15	489	2.4
275	427603	4517975.7	34	1	558	2.8
275	427603	4517975.7	34	7	534	2.7
275	427603	4517975.7	34	15	490	2.5
276	427281	4517987.7	33	1	555	2.8
276	427281	4517987.7	33	7	537	2.7
276	427281	4517987.7	33	15	506	2.5
277	426306	4518342	34	1	568	2.8
277	426306	4518342	34	7	552	2.8
277	426306	4518342	34	15	478	2.4
278	425446	4518523.1	31	1	547	2.7
278	425446	4518523.1	31	7	532	2.7
278	425446	4518523.1	31	15	476	2.4
279	429070	4517872.6	15	1	560	2.8
279	429070	4517872.6	15	7	501	2.5
279	429070	4517872.6	15	12	488	2.4
280	429212	4517974.5	12	1	533	2.7
280	429212	4517974.5	12	9	516	2.6
281	429399	4518113.7	4.7	1	589	2.9
281	429399	4518113.7	4.7	3	568	2.8
282	429508	4518155.9	3.1	1	2439	12.2
283	429484	4518241.7	2.4	1	4408	22.0
284	429422	4518210	3.7	1	815	4.1
285	429229	4518176.4	6.4	1	621	3.1
285	429229	4518176.4	6.4	5	566	2.8
286	429283	4518351.3	3.5	1	831	4.2
287	429055	4518283.5	7.4	1	658	3.3
287	429055	4518283.5	7.4	5	574	2.9
288	428901	4518111.8	12	1	604	3.0
288	428901	4518111.8	12	9	527	2.6
289	428951	4518506.5	5	1	813	4.1
290	428982	4518610.6	3.3	1	882	4.4
291	428682	4518488	7.7	1	746	3.7
291	428682	4518488	7.7	5	701	3.5
292	428308	4518521.6	9.5	1	594	3.0
292	428308	4518521.6	9.5	8	489	2.4
293	427923	4518698.6	7.4	1	546	2.7
293	427923	4518698.6	7.4	5	504	2.5
294	427715	4518733.9	8.5	1	554	2.8
294	427715	4518733.9	8.5	6	512	2.6
295	427378	4518723.9	9.4	1	505	2.5

295	427378	4518723.9	9.4	7	500	2.5
296	427178	4518709.2	11	1	545	2.7
296	427178	4518709.2	11	8	519	2.6
297	426916	4518829.5	8.1	1	535	2.7
297	426916	4518829.5	8.1	6	510	2.5
298	426470	4518942.7	7.5	1	533	2.7
298	426470	4518942.7	7.5	6	510	2.5
299	426199	4518920.9	9.8	1	512	2.6
299	426199	4518920.9	9.8	8	502	2.5
300	426002	4518961.8	8.1	1	506	2.5
300	426002	4518961.8	8.1	6	505	2.5
301	425646	4518908.7	12	1	505	2.5
301	425646	4518908.7	12	8	501	2.5
302	425294	4519051.1	18	1	508	2.5
302	425294	4519051.1	18	8	507	2.5
303	425291	4519173.2	13	1	511	2.6
303	425291	4519173.2	13	8	516	2.6
304	425040	4519273.4	17	1	518	2.6
304	425040	4519273.4	17	8	496	2.5
305	425053	4519032.4	24	1	506	2.5
305	425053	4519032.4	24	8	499	2.5
306	425566	4519692.2	3.2	1	533	2.7
307	425370	4519689.8	3	1	541	2.7
308	424984	4519922.4	9	1	514	2.6
308	424984	4519922.4	9	6	497	2.5
309	424929	4520090.6	4.3	1	501	2.5
310	424789	4520115.3	2.8	1	516	2.6
311	424662	4520163.2	3	1	509	2.5
312	424531	4520180.1	2.9	1	516	2.6
313	424560	4520052.1	6.1	1	520	2.6
314	424729	4519970.5	8.7	1	519	2.6
314	424729	4519970.5	8.7	6	502	2.5
315	423066	4514466.6	8	1	590	2.9
315	423066	4514466.6	8	8	660	3.3
316	423084	4514510.7	7	6.7	2283	11.4
317	423361	4514627.3	16	1	610	3.0
317	423361	4514627.3	16	15	598	3.0
318	423358	4514809.2	9	1	589	2.9
318	423358	4514809.2	9	8	583	2.9
319	423410	4515002.1	8.5	1	582	2.9
319	423410	4515002.1	8.5	7.5	582	2.9
320	423361	4515071.6	6	1	549	2.7
320	423361	4515071.6	6	5	549	2.7
321	423399	4515334.8	10.6	1	574	2.9
321	423399	4515334.8	10.6	9	552	2.8
322	423306	4515367.4	8.7	1	553	2.8
322	423306	4515367.4	8.7	8	556	2.8

323	423236	4515615.4	8.5	1	577	2.9
323	423236	4515615.4	8.5	8	579	2.9
324	423529	4515722.2	13.5	1	592	3.0
324	423529	4515722.2	13.5	12	543	2.7
325	423209	4515858.3	6	1	690	3.5
325	423209	4515858.3	6	4.5	681	3.4
326	422923	4516060.4	5	1	761	3.8
326	422923	4516060.4	5	4.5	767	3.8
327	422910	4516071.1	5	1	796	4.0
327	422910	4516071.1	5	4.5	750	3.8
328	422836	4516066.3	5	1	789	3.9
328	422836	4516066.3	5	4	799	4.0
329	422805	4516043.6	7	1	829	4.1
329	422805	4516043.6	7	6	1676	8.4
330	422793	4515994.2	7.5	1	896	4.5
330	422793	4515994.2	7.5	6	842	4.2
331	422763	4516027.1	7	1	953	4.8
331	422763	4516027.1	7	6	825	4.1
332	422735	4515947.7	7	1	949	4.7
332	422735	4515947.7	7	5	894	4.5
333	422720	4515887.5	6.5	1	945	4.7
333	422720	4515887.5	6.5	5	1321	6.6
334	422587	4515961.2	4.5	1	958	4.8
335	422596	4516003.1	5	1	903	4.5
335	422596	4516003.1	5	4	796	4.0
336	422860	4515838	8.1	1	893	4.5
336	422860	4515838	8.1	6	844	4.2
337	422953	4515879.6	7.5	1	902	4.5
337	422953	4515879.6	7.5	5	676	3.4
338	423148	4515869.1	6.5	1	828	4.1
338	423148	4515869.1	6.5	4.5	681	3.4
339	423040	4515721.8	10.2	1	854	4.3
339	423040	4515721.8	10.2	7.5	675	3.4
340	423113	4515647.6	7	1	1055	5.3
340	423113	4515647.6	7	5	865	4.3
341	423112	4515621.7	6.6	1	1138	5.7
342	423656	4515725	20	1	588	2.9
342	423656	4515725	20	10	545	2.7
343	423382	4515969.8	12.5	1	589	2.9
343	423382	4515969.8	12.5	10	571	2.9
344	423277	4516121.9	12	1	608	3.0
344	423277	4516121.9	12	10	584	2.9
345	423205	4516255.9	11.4	1	601	3.0
345	423205	4516255.9	11.4	10	587	2.9
346	423143	4516350.9	10.5	1	590	2.9
346	423143	4516350.9	10.5	9.5	595	3.0
347	423065	4516506	11	1	606	3.0

347	423065	4516506	11	10	603	3.0
348	423001	4516633.3	10	1	597	3.0
348	423001	4516633.3	10	9	573	2.9
349	422999	4516833.1	32	1	588	2.9
349	422999	4516833.1	32	10	576	2.9
350	423027	4516986	41	1	582	2.9
350	423027	4516986	41	10	575	2.9
351	423125	4517092.7	48	1	584	2.9
351	423125	4517092.7	48	10	569	2.8
352	422902	4517228.2	42	1	583	2.9
352	422902	4517228.2	42	10	572	2.9
353	422820	4517170.3	16	1	582	2.9
353	422820	4517170.3	16	10	583	2.9
354	422823	4517303.5	20	1	583	2.9
354	422823	4517303.5	20	10	543	2.7
355	422849	4517440.8	23	1	581	2.9
355	422849	4517440.8	23	10	558	2.8
356	422817	4517561.1	18	1	584	2.9
356	422817	4517561.1	18	10	551	2.8
357	422763	4517561.6	14.5	1	581	2.9
357	422763	4517561.6	14.5	10	560	2.8
358	423017	4517391.4	47	1	589	2.9
358	423017	4517391.4	47	10	550	2.7
359	422980	4517512.8	44	1	580	2.9
359	422980	4517512.8	44	10	548	2.7
360	430383	4516463.5	6.5	1	447	2.2
360	430383	4516463.5	6.5	6	447	2.2
361	430260	4516612.3	8	1	470	2.4
361	430260	4516612.3	8	7	470	2.4
362	430067	4516526.4	14.5	1	547	2.7
362	430067	4516526.4	14.5	11	547	2.7
363	430320	4516755	2	1	1012	5.1
364	430398	4516663.2	3	1	571	2.9
365	429926	4516413.4	1	1	450	2.3
366	430166	4516287.9	12.5	1	432	2.2
367	429746	4516238.6	14	1	430	2.2
368	429844	4515900.2	22	1	430	2.2
369	429493	4516000.1	22	1	431	2.2
370	429580	4515667.3	28	1	431	2.2
371	429231	4515991.5	20	1	429	2.1
372	429067	4516147.4	30	1	434	2.2
373	428993	4516324.6	22	1	439	2.2
374	429014	4516566.4	13	1	440	2.2
375	429014	4516566.4	13	12	440	2.2
376	429156	4516716.1	15	1	444	2.2
377	429264	4516736.1	9	1	456	2.3
377	429264	4516736.1	9	8	456	2.3

378	428610	4516968.9	54	1	435	2.2
379	429297	4516955.6	20	1	480	2.4
380	429491	4516930.5	13	1	570	2.9
380	429491	4516930.5	13	10	570	2.9
381	429607	4516825	7	1	571	2.9
382	429742	4516724.9	8.5	1	613	3.1
383	429742	4516724.9	8.5	7.5	613	3.1
384	429713	4516909.5	7.5	1	590	3.0
385	429925	4517030.7	5	1	598	3.0
386	430101	4516945.8	3.5	1	645	3.2
387	430158	4516949.7	3.5	1	697	3.5
388	430173	4516932.9	3	1	762	3.8
389	430143	4517075.3	3	1	695	3.5
390	430210	4517111.3	2	1	814	4.1
391	430174	4517200.4	2.5	1	815	4.1
392	430079	4517321.2	4.5	1	556	2.8
393	430047	4517531.3	3.7	1	624	3.1
394	429935	4517491.3	5	1	523	2.6
395	429794	4517350.6	9	1	551	2.8
396	429548	4517243	12	1	532	2.7
397	429395	4517365.5	20	1	490	2.5
398	429067	4517339.7	23	1	449	2.2
399	429139	4517683.2	20	1	456	2.3
400	429301	4517824.9	10	1	475	2.4
401	429442	4517965.6	7	1	551	2.8
402	429604	4518012.9	3.5	1	766	3.8
403	429598	4518088.5	2.5	1	655	3.3
404	429713	4517889.8	3	1	1823	9.1
405	429722	4517910.8	2	1	1508	7.5
406	429767	4517721.6	7	1	525	2.6
407	429789	4517717	2.5	1	492	2.5
CF01	431479	4518414	-	-	36041	-
CF02	431588	4518570	-	-	22009	-
CF03	431270	4520135	-	-	19888	-
CF04	429495	4518411	-	-	82167	-
CF05	429540	4518436	-	-	126794	-
CF06	429513	4521799	-	-	5883	-
CF07	430627	4521138	-	-	7229	-
CF08	429288	4521042	-	-	781448	-
CF09	430820	4521335	-	-	3828	-
CF10	430220	4520007	-	-	798730	-
CF11	430254	4519984	-	-	836180	-
CF12	431350	4519613	-	-	73553	-
CF13	428473	4520279	-	-	217470	-
CF15	426673	4523998	-	-	1720	-
CF16	425538	4520154	-	-	31688	-
CF17	422990	4520347	-	-	5415	-

CF18	425591	4520818	-	-	35876	-
CF19	425923	4523376	-	-	22667	-
CF20	431993	4518392	-	-	18493	-
CF21	423442	4521220	-	-	85822	-
CF22	423951	4522018	-	-	92257	-
CF23	422092	4520008	-	-	37351	-
CF24	422085	4520080	-	-	49386	-
CF25	428290	4521610	-	-	19670	-
CF26	422224	4520568	-	-	52143	-
CF27	422399	4520443	-	-	24132	-
CF28	421576	4518931	-	-	23719	-
CF29	422854	4520288	-	-	61306	-
CF30	422934	4522349	-	-	41162	-
CF31	422270	4522360	-	-	5168	-
CF32	426470	4523703	-	-	6227	-
CF33	428156	4523197	-	-	7452	-
CF34	425248	4525288	-	-	1197	-
CF35	425473	4525921	-	-	42540	-
CF36	426102	4526828	-	-	29854	-
CF37	428230	4526188	-	-	13354	-
CF38	424907	4526562	-	-	17322	-
CF39	428628	4526704	-	-	25340	-
CF40	428535	4526327	-	-	9382	-
CF41	424880	4527098	-	-	993	-
CF42	421167	4524564	-	-	334	-
CF43	424180	4524642	-	-	1733	-
CF44	421116	4523218	-	-	15915	-
CF45	422291	4523389	-	-	474	-
CF46	421944	4523450	-	-	1870	-
CF47	422150	4525423	-	-	18022	-
CF48	424590	4522610	-	-	17898	-
CF49	422399	4520443	-	-	14686	-
CF50	425867	4519829	-	-	56938	-
CF51	425867	4519829	-	-	163192	-
CF52	423130	4521450	-	-	106121	-
CF53	423888	4521240	-	-	39039	-
CF54	422187	4519790	-	-	345541	-
CF55	428120	4524113	-	-	18264	-
CF56	425904	4527179	-	-	5226	-
CF57	423378	4521605	-	-	48652	-
CF58	423191	4523308	-	-	2150	-
CF59	425551	4521700	-	-	8582	-
CF60	420878	4521902	-	-	1172	-
CF61	420947	4520709	-	-	14545	-
CF62	421038	4521685	-	-	7532	-
CF63A	421845	4526093	-	-	4373	-
CF64	420701	4519764	-	-	132190	-

CF65	420713	4522640	-	-	10242	-
CF66	420308	4521050	-	-	8339	-
CF67	420566	4521099	-	-	14801	-
CF68	426603	4519873	-	-	180219	-
CF69	426662	4526255	-	-	80039	-
CF70	426557	4520976	-	-	482281	-
CF72	428087	4520160	-	-	144677	-
CF74	422533	4521056	-	-	7881	-
CF75	427427	4519870	-	-	867961	-
CF76	429114	4519924	-	-	25334	-
CF77	428670	4519730	-	-	19702	-
CF78	421795	4518144	-	-	597035	-
CF79	423876	4520537	-	-	1290	-
CF80	429110	4521088	-	-	392103	-
CF81	421650	4518322	-	-	5090	-
CF82	427122	4519107	-	-	5749	-
CF83	422988	4520348	-	-	317	-
CF84	425832	4524362	-	-	21429	-
CF85	425482	4523338	-	-	12145	-
CF86	420671	4522364	-	-	31521	-

ı groundwaters after Caliro et al. (2025b). Reported errors for pCO_2 are 1σ uncertainties. The depth is
› the atmospheric equilibrium pCO_2 value of 420 µm.

Log_{10} (pCO2)	Excess carbon (mol/kg)	Excess carbon (µmol/kg)	Type	Reference
2.7	4.2E-05	41.7	Seawater	This work
2.7	3.1E-05	31.3	Seawater	This work
2.6	1.5E-05	14.9	Seawater	This work
2.7	4.9E-05	48.8	Seawater	This work
2.7	4.8E-05	48.3	Seawater	This work
2.7	5.1E-05	51.1	Seawater	This work
2.7	4.9E-05	49.3	Seawater	This work
3.2	2.6E-04	257.7	Seawater	This work
2.7	5.3E-05	52.9	Seawater	This work
2.8	7.5E-05	75.5	Seawater	This work
2.7	5.6E-05	56.1	Seawater	This work
2.7	5.6E-05	56.1	Seawater	This work
2.7	5.3E-05	53.4	Seawater	This work
2.7	5.6E-05	55.6	Seawater	This work
2.7	5.8E-05	58.3	Seawater	This work
2.7	5.8E-05	57.8	Seawater	This work
2.7	5.7E-05	57.4	Seawater	This work
2.8	7.6E-05	76.3	Seawater	This work
2.7	5.7E-05	57.4	Seawater	This work
2.7	2.2E-05	22.5	Seawater	This work
2.6	1.8E-06	1.8	Seawater	This work
2.7	3.1E-05	31.3	Seawater	This work
2.6	3.0E-06	3.0	Seawater	This work
2.6	8.2E-06	8.2	Seawater	This work
2.6	1.2E-06	1.2	Seawater	This work
2.6	5.9E-07	0.6	Seawater	This work
2.9	1.6E-04	160.1	Seawater	This work
2.7	1.8E-05	18.2	Seawater	This work
2.7	6.5E-05	64.8	Seawater	This work
2.7	1.8E-05	18.2	Seawater	This work
2.6	1.0E-05	10.4	Seawater	This work
2.7	3.3E-05	32.8	Seawater	This work
2.7	2.8E-05	27.7	Seawater	This work
2.7	4.6E-05	45.5	Seawater	This work
2.7	3.6E-05	36.3	Seawater	This work
2.7	5.1E-05	51.1	Seawater	This work
2.7	5.1E-05	51.1	Seawater	This work
2.7	5.9E-05	59.2	Seawater	This work
2.6	1.2E-06	1.2	Seawater	This work
2.7	2.8E-05	27.7	Seawater	This work
2.7	3.1E-05	30.8	Seawater	This work
2.6	9.9E-06	9.9	Seawater	This work

2.6	1.8E-06	1.8	Seawater	This work
2.6	9.3E-06	9.3	Seawater	This work
2.6	8.7E-06	8.7	Seawater	This work
2.6	7.6E-06	7.6	Seawater	This work
2.6	4.1E-06	4.1	Seawater	This work
2.6	4.1E-06	4.1	Seawater	This work
2.6	4.7E-06	4.7	Seawater	This work
2.6	6.5E-06	6.5	Seawater	This work
2.6	1.3E-05	13.2	Seawater	This work
2.7	1.7E-05	17.1	Seawater	This work
2.6	1.3E-05	12.7	Seawater	This work
2.7	2.1E-05	20.9	Seawater	This work
2.7	3.0E-05	30.3	Seawater	This work
2.6	1.4E-05	14.4	Seawater	This work
2.6	1.1E-05	11.0	Seawater	This work
2.6	1.4E-05	14.4	Seawater	This work
2.7	1.6E-05	16.0	Seawater	This work
2.7	2.7E-05	26.7	Seawater	This work
2.7	3.2E-05	31.8	Seawater	This work
2.7	3.4E-05	34.3	Seawater	This work
2.7	3.3E-05	32.8	Seawater	This work
2.7	2.2E-05	22.5	Seawater	This work
2.7	1.9E-05	18.7	Seawater	This work
2.7	1.8E-05	17.6	Seawater	This work
2.7	1.9E-05	19.3	Seawater	This work
2.6	1.0E-05	10.4	Seawater	This work
2.7	1.9E-05	18.7	Seawater	This work
2.6	9.3E-06	9.3	Seawater	This work
2.7	1.7E-05	16.6	Seawater	This work
2.6	4.1E-06	4.1	Seawater	This work
2.7	1.8E-05	18.2	Seawater	This work
2.6	3.5E-06	3.5	Seawater	This work
2.7	3.6E-05	35.8	Seawater	This work
2.6	8.7E-06	8.7	Seawater	This work
2.6	1.3E-05	12.7	Seawater	This work
2.7	3.0E-05	30.3	Seawater	This work
2.6	8.2E-06	8.2	Seawater	This work
2.7	3.3E-05	32.8	Seawater	This work
2.7	1.7E-05	16.6	Seawater	This work
2.7	3.3E-05	32.8	Seawater	This work
2.7	1.8E-05	17.6	Seawater	This work
2.7	4.4E-05	43.6	Seawater	This work
2.7	2.7E-05	27.2	Seawater	This work
2.6	1.8E-06	1.8	Seawater	This work
2.7	3.8E-05	37.8	Seawater	This work
2.7	2.0E-05	20.4	Seawater	This work
2.6	7.0E-06	7.0	Seawater	This work

2.7	2.9E-05	29.3	Seawater	This work
2.7	2.6E-05	25.7	Seawater	This work
2.6	4.7E-06	4.7	Seawater	This work
2.7	3.8E-05	38.3	Seawater	This work
2.7	5.2E-05	51.6	Seawater	This work
2.7	3.7E-05	36.8	Seawater	This work
2.7	2.4E-05	23.6	Seawater	This work
2.6	1.3E-05	13.2	Seawater	This work
2.7	3.6E-05	36.3	Seawater	This work
2.7	2.5E-05	24.6	Seawater	This work
2.6	5.3E-06	5.3	Seawater	This work
2.7	3.7E-05	37.3	Seawater	This work
2.7	4.3E-05	42.7	Seawater	This work
2.7	2.7E-05	26.7	Seawater	This work
2.7	3.8E-05	38.3	Seawater	This work
2.7	5.5E-05	55.2	Seawater	This work
2.7	3.2E-05	32.3	Seawater	This work
2.7	3.6E-05	35.8	Seawater	This work
2.7	4.6E-05	46.0	Seawater	This work
2.7	2.2E-05	22.5	Seawater	This work
2.7	4.2E-05	41.7	Seawater	This work
2.6	1.4E-05	14.4	Seawater	This work
2.7	4.1E-05	40.7	Seawater	This work
2.6	1.4E-05	13.8	Seawater	This work
2.7	4.1E-05	40.7	Seawater	This work
2.7	1.8E-05	17.6	Seawater	This work
2.7	3.6E-05	36.3	Seawater	This work
2.7	2.1E-05	20.9	Seawater	This work
2.6	3.5E-06	3.5	Seawater	This work
2.7	4.8E-05	48.3	Seawater	This work
2.6	9.3E-06	9.3	Seawater	This work
2.7	4.7E-05	46.9	Seawater	This work
2.7	3.3E-05	33.3	Seawater	This work
2.6	1.1E-05	11.0	Seawater	This work
2.7	4.5E-05	45.0	Seawater	This work
2.8	1.2E-04	117.9	Seawater	This work
2.8	9.3E-05	92.7	Seawater	This work
2.8	1.0E-04	101.2	Seawater	This work
2.8	1.1E-04	105.6	Seawater	This work
2.8	7.6E-05	75.9	Seawater	This work
2.8	1.1E-04	111.6	Seawater	This work
2.8	7.9E-05	79.5	Seawater	This work
2.8	9.2E-05	91.6	Seawater	This work
2.8	7.8E-05	78.3	Seawater	This work
2.8	8.5E-05	84.9	Seawater	This work
2.8	8.2E-05	81.8	Seawater	This work
2.8	1.2E-04	115.4	Seawater	This work

2.8	8.6E-05	86.0	Seawater	This work
2.9	1.2E-04	122.0	Seawater	This work
2.9	1.3E-04	129.1	Seawater	This work
2.8	1.1E-04	109.9	Seawater	This work
2.7	6.9E-05	69.4	Seawater	This work
2.8	8.4E-05	84.5	Seawater	This work
2.8	7.6E-05	76.3	Seawater	This work
2.7	6.9E-05	69.4	Seawater	This work
2.7	6.5E-05	65.2	Seawater	This work
2.7	6.0E-05	60.0	Seawater	This work
2.7	5.3E-05	52.9	Seawater	This work
2.7	6.2E-05	61.8	Seawater	This work
2.7	6.0E-05	60.5	Seawater	This work
2.7	4.9E-05	48.8	Seawater	This work
2.7	6.0E-05	60.5	Seawater	This work
2.7	6.1E-05	61.3	Seawater	This work
2.7	6.0E-05	60.5	Seawater	This work
2.8	7.5E-05	75.5	Seawater	This work
2.7	5.9E-05	59.2	Seawater	This work
2.7	3.4E-05	33.8	Seawater	This work
2.8	8.7E-05	87.5	Seawater	This work
2.7	4.9E-05	49.3	Seawater	This work
2.7	4.2E-05	41.7	Seawater	This work
2.8	8.9E-05	88.6	Seawater	This work
2.7	4.7E-05	47.4	Seawater	This work
2.7	2.8E-05	28.3	Seawater	This work
2.8	9.0E-05	90.5	Seawater	This work
2.7	4.3E-05	42.7	Seawater	This work
2.7	3.2E-05	32.3	Seawater	This work
2.8	8.1E-05	81.4	Seawater	This work
2.7	4.5E-05	45.0	Seawater	This work
2.7	5.2E-05	52.5	Seawater	This work
2.8	1.2E-04	117.9	Seawater	This work
3.1	2.2E-04	225.0	Seawater	This work
2.9	1.5E-04	152.5	Seawater	This work
2.8	1.2E-04	117.3	Seawater	This work
2.7	6.6E-05	66.5	Seawater	This work
2.7	6.5E-05	64.8	Seawater	This work
2.7	5.5E-05	54.7	Seawater	This work
2.7	6.4E-05	64.3	Seawater	This work
2.8	7.5E-05	75.1	Seawater	This work
2.7	5.2E-05	52.0	Seawater	This work
2.8	7.9E-05	79.5	Seawater	This work
2.7	6.7E-05	67.3	Seawater	This work
2.7	4.9E-05	48.8	Seawater	This work
2.7	6.6E-05	66.5	Seawater	This work
2.7	4.6E-05	45.5	Seawater	This work

2.7	3.7E-05	37.3	Seawater	This work
2.7	6.4E-05	64.3	Seawater	This work
2.7	5.8E-05	57.8	Seawater	This work
2.7	2.8E-05	27.7	Seawater	This work
2.7	6.5E-05	64.8	Seawater	This work
2.7	5.2E-05	52.0	Seawater	This work
2.7	3.7E-05	37.3	Seawater	This work
2.7	6.9E-05	68.6	Seawater	This work
2.7	5.8E-05	58.3	Seawater	This work
2.7	3.8E-05	37.8	Seawater	This work
2.7	6.7E-05	67.3	Seawater	This work
2.7	6.0E-05	59.6	Seawater	This work
2.7	4.6E-05	45.5	Seawater	This work
2.8	7.3E-05	72.7	Seawater	This work
2.7	6.6E-05	66.0	Seawater	This work
2.7	3.2E-05	31.8	Seawater	This work
2.7	6.4E-05	63.9	Seawater	This work
2.7	5.7E-05	57.4	Seawater	This work
2.7	3.1E-05	30.8	Seawater	This work
2.7	6.9E-05	69.3	Seawater	This work
2.7	4.3E-05	42.9	Seawater	This work
2.7	3.7E-05	36.9	Seawater	This work
2.7	5.8E-05	58.0	Seawater	This work
2.7	5.0E-05	50.2	Seawater	This work
2.8	8.1E-05	80.9	Seawater	This work
2.8	7.2E-05	72.5	Seawater	This work
3.4	3.5E-04	345.8	Seawater	This work
3.6	4.4E-04	444.1	Seawater	This work
2.9	1.5E-04	151.6	Seawater	This work
2.8	9.3E-05	93.0	Seawater	This work
2.8	7.2E-05	71.9	Seawater	This work
2.9	1.6E-04	155.6	Seawater	This work
2.8	1.1E-04	105.8	Seawater	This work
2.8	7.5E-05	75.3	Seawater	This work
2.8	8.7E-05	86.9	Seawater	This work
2.7	5.5E-05	55.3	Seawater	This work
2.9	1.5E-04	151.3	Seawater	This work
2.9	1.7E-04	167.9	Seawater	This work
2.9	1.3E-04	133.2	Seawater	This work
2.8	1.2E-04	119.9	Seawater	This work
2.8	8.3E-05	83.0	Seawater	This work
2.7	3.7E-05	37.3	Seawater	This work
2.7	6.3E-05	63.4	Seawater	This work
2.7	4.5E-05	44.5	Seawater	This work
2.7	6.7E-05	66.9	Seawater	This work
2.7	4.8E-05	48.3	Seawater	This work
2.7	4.5E-05	44.9	Seawater	This work

2.7	4.3E-05	42.5	Seawater	This work
2.7	6.3E-05	62.9	Seawater	This work
2.7	5.2E-05	51.7	Seawater	This work
2.7	5.9E-05	58.8	Seawater	This work
2.7	4.7E-05	47.3	Seawater	This work
2.7	5.8E-05	57.9	Seawater	This work
2.7	4.7E-05	47.3	Seawater	This work
2.7	4.8E-05	48.4	Seawater	This work
2.7	4.4E-05	43.7	Seawater	This work
2.7	4.5E-05	45.4	Seawater	This work
2.7	4.5E-05	45.1	Seawater	This work
2.7	4.5E-05	45.1	Seawater	This work
2.7	4.3E-05	43.2	Seawater	This work
2.7	4.7E-05	46.6	Seawater	This work
2.7	4.6E-05	46.2	Seawater	This work
2.7	4.8E-05	47.9	Seawater	This work
2.7	5.0E-05	50.2	Seawater	This work
2.7	5.1E-05	51.2	Seawater	This work
2.7	4.1E-05	40.6	Seawater	This work
2.7	4.5E-05	45.4	Seawater	This work
2.7	4.2E-05	42.4	Seawater	This work
2.7	5.8E-05	58.0	Seawater	This work
2.7	6.1E-05	61.4	Seawater	This work
2.7	4.9E-05	49.5	Seawater	This work
2.7	4.1E-05	41.1	Seawater	This work
2.7	4.3E-05	43.4	Seawater	This work
2.7	5.0E-05	50.1	Seawater	This work
2.7	4.7E-05	46.9	Seawater	This work
2.7	5.0E-05	50.1	Seawater	This work
2.7	5.2E-05	52.0	Seawater	This work
2.7	5.2E-05	51.6	Seawater	This work
2.7	4.3E-05	43.4	Seawater	This work
2.8	8.1E-05	81.3	Seawater	This work
2.8	1.1E-04	106.6	Seawater	This work
3.4	3.4E-04	335.2	Seawater	This work
2.8	8.9E-05	88.9	Seawater	This work
2.8	8.5E-05	84.6	Seawater	This work
2.8	8.1E-05	81.2	Seawater	This work
2.8	7.9E-05	78.8	Seawater	This work
2.8	7.8E-05	78.1	Seawater	This work
2.8	7.8E-05	78.2	Seawater	This work
2.7	6.5E-05	64.7	Seawater	This work
2.7	6.5E-05	64.9	Seawater	This work
2.8	7.5E-05	74.9	Seawater	This work
2.7	6.6E-05	66.0	Seawater	This work
2.7	6.6E-05	66.4	Seawater	This work
2.7	6.8E-05	67.8	Seawater	This work

2.8	7.6E-05	76.3	Seawater	This work
2.8	7.7E-05	77.2	Seawater	This work
2.8	8.2E-05	82.1	Seawater	This work
2.7	6.2E-05	62.0	Seawater	This work
2.8	1.2E-04	116.4	Seawater	This work
2.8	1.1E-04	113.4	Seawater	This work
2.9	1.4E-04	137.5	Seawater	This work
2.9	1.4E-04	139.1	Seawater	This work
2.9	1.5E-04	146.9	Seawater	This work
2.9	1.3E-04	134.3	Seawater	This work
2.9	1.5E-04	145.0	Seawater	This work
2.9	1.5E-04	147.5	Seawater	This work
2.9	1.6E-04	155.2	Seawater	This work
3.2	2.8E-04	284.9	Seawater	This work
3.0	1.7E-04	170.9	Seawater	This work
2.9	1.6E-04	158.4	Seawater	This work
3.0	1.8E-04	183.2	Seawater	This work
2.9	1.5E-04	154.3	Seawater	This work
3.0	1.8E-04	182.3	Seawater	This work
3.0	1.7E-04	170.6	Seawater	This work
3.0	1.8E-04	181.4	Seawater	This work
3.1	2.4E-04	244.0	Seawater	This work
3.0	1.8E-04	184.3	Seawater	This work
3.0	1.7E-04	172.5	Seawater	This work
2.9	1.5E-04	146.8	Seawater	This work
3.0	1.7E-04	170.3	Seawater	This work
2.9	1.6E-04	158.8	Seawater	This work
3.0	1.7E-04	172.3	Seawater	This work
2.8	1.1E-04	111.9	Seawater	This work
2.9	1.5E-04	154.9	Seawater	This work
2.8	1.1E-04	113.4	Seawater	This work
2.9	1.6E-04	161.3	Seawater	This work
2.8	1.1E-04	111.6	Seawater	This work
3.0	2.0E-04	202.8	Seawater	This work
2.9	1.6E-04	163.9	Seawater	This work
3.1	2.2E-04	217.1	Seawater	This work
2.8	8.1E-05	80.5	Seawater	This work
2.7	6.3E-05	62.9	Seawater	This work
2.8	8.1E-05	81.0	Seawater	This work
2.8	7.4E-05	74.0	Seawater	This work
2.8	8.8E-05	88.3	Seawater	This work
2.8	7.9E-05	79.2	Seawater	This work
2.8	8.5E-05	85.5	Seawater	This work
2.8	8.0E-05	80.1	Seawater	This work
2.8	8.1E-05	81.3	Seawater	This work
2.8	8.3E-05	83.2	Seawater	This work
2.8	8.7E-05	87.4	Seawater	This work

2.8	8.6E-05	86.5	Seawater	This work
2.8	8.4E-05	83.9	Seawater	This work
2.8	7.5E-05	74.6	Seawater	This work
2.8	8.1E-05	80.6	Seawater	This work
2.8	7.6E-05	76.0	Seawater	This work
2.8	7.8E-05	78.4	Seawater	This work
2.8	7.5E-05	75.4	Seawater	This work
2.8	7.9E-05	79.0	Seawater	This work
2.8	7.3E-05	73.2	Seawater	This work
2.8	7.9E-05	78.6	Seawater	This work
2.8	7.4E-05	74.2	Seawater	This work
2.8	7.8E-05	78.2	Seawater	This work
2.8	7.9E-05	78.7	Seawater	This work
2.8	7.9E-05	78.8	Seawater	This work
2.7	6.2E-05	62.2	Seawater	This work
2.8	7.8E-05	78.0	Seawater	This work
2.7	6.9E-05	68.5	Seawater	This work
2.8	7.9E-05	79.2	Seawater	This work
2.7	6.6E-05	65.6	Seawater	This work
2.8	7.8E-05	78.1	Seawater	This work
2.7	7.0E-05	69.6	Seawater	This work
2.8	8.1E-05	81.2	Seawater	This work
2.7	6.5E-05	65.1	Seawater	This work
2.8	7.8E-05	77.5	Seawater	This work
2.7	6.4E-05	64.3	Seawater	This work
2.7	1.5E-05	15.5	Seawater	This work
2.7	1.5E-05	15.5	Seawater	This work
2.7	2.8E-05	27.7	Seawater	This work
2.7	2.8E-05	27.7	Seawater	This work
2.7	6.4E-05	63.9	Seawater	This work
2.7	6.4E-05	63.9	Seawater	This work
3.0	1.9E-04	194.9	Seawater	This work
2.8	7.4E-05	73.9	Seawater	This work
2.7	1.7E-05	17.1	Seawater	This work
2.6	7.0E-06	7.0	Seawater	This work
2.6	5.9E-06	5.9	Seawater	This work
2.6	5.9E-06	5.9	Seawater	This work
2.6	6.4E-06	6.4	Seawater	This work
2.6	6.4E-06	6.4	Seawater	This work
2.6	5.3E-06	5.3	Seawater	This work
2.6	8.2E-06	8.2	Seawater	This work
2.6	1.1E-05	11.0	Seawater	This work
2.6	1.2E-05	11.6	Seawater	This work
2.6	1.2E-05	11.6	Seawater	This work
2.6	1.4E-05	13.8	Seawater	This work
2.7	2.0E-05	20.4	Seawater	This work
2.7	2.0E-05	20.4	Seawater	This work

2.6	8.7E-06	8.7	Seawater	This work
2.7	3.3E-05	32.8	Seawater	This work
2.8	7.3E-05	73.5	Seawater	This work
2.8	7.3E-05	73.5	Seawater	This work
2.8	7.4E-05	73.9	Seawater	This work
2.8	9.0E-05	90.1	Seawater	This work
2.8	9.0E-05	90.1	Seawater	This work
2.8	8.1E-05	81.4	Seawater	This work
2.8	8.4E-05	84.5	Seawater	This work
2.8	1.0E-04	101.5	Seawater	This work
2.8	1.2E-04	118.6	Seawater	This work
2.9	1.4E-04	137.7	Seawater	This work
2.8	1.2E-04	117.9	Seawater	This work
2.9	1.5E-04	151.4	Seawater	This work
2.9	1.5E-04	151.7	Seawater	This work
2.7	6.8E-05	67.7	Seawater	This work
2.8	9.4E-05	94.1	Seawater	This work
2.7	5.3E-05	53.4	Seawater	This work
2.7	6.6E-05	65.6	Seawater	This work
2.7	5.7E-05	57.4	Seawater	This work
2.7	3.8E-05	37.8	Seawater	This work
2.7	1.7E-05	16.6	Seawater	This work
2.7	2.0E-05	20.4	Seawater	This work
2.7	3.0E-05	30.3	Seawater	This work
2.7	6.6E-05	65.6	Seawater	This work
2.9	1.4E-04	138.8	Seawater	This work
2.8	1.0E-04	104.9	Seawater	This work
3.3	3.0E-04	298.8	Seawater	This work
3.2	2.7E-04	267.1	Seawater	This work
2.7	5.4E-05	54.3	Seawater	This work
2.7	3.9E-05	38.8	Seawater	This work
4.6	-	-	Groundwater	Caliro et al. (2025b)
4.3	-	-	Groundwater	Caliro et al. (2025b)
4.3	-	-	Groundwater	Caliro et al. (2025b)
4.9	-	-	Groundwater	Caliro et al. (2025b)
5.1	-	-	Groundwater	Caliro et al. (2025b)
3.8	-	-	Groundwater	Caliro et al. (2025b)
3.9	-	-	Groundwater	Caliro et al. (2025b)
5.9	-	-	Groundwater	Caliro et al. (2025b)
3.6	-	-	Groundwater	Caliro et al. (2025b)
5.9	-	-	Groundwater	Caliro et al. (2025b)
5.9	-	-	Groundwater	Caliro et al. (2025b)
4.9	-	-	Groundwater	Caliro et al. (2025b)
5.3	-	-	Groundwater	Caliro et al. (2025b)
3.2	-	-	Groundwater	Caliro et al. (2025b)
4.5	-	-	Groundwater	Caliro et al. (2025b)
3.7	-	-	Groundwater	Caliro et al. (2025b)

4.6	-	-	Groundwater	Caliro et al. (2025b)
4.4	-	-	Groundwater	Caliro et al. (2025b)
4.3	-	-	Groundwater	Caliro et al. (2025b)
4.9	-	-	Groundwater	Caliro et al. (2025b)
5.0	-	-	Groundwater	Caliro et al. (2025b)
4.6	-	-	Groundwater	Caliro et al. (2025b)
4.7	-	-	Groundwater	Caliro et al. (2025b)
4.3	-	-	Groundwater	Caliro et al. (2025b)
4.7	-	-	Groundwater	Caliro et al. (2025b)
4.4	-	-	Groundwater	Caliro et al. (2025b)
4.4	-	-	Groundwater	Caliro et al. (2025b)
4.8	-	-	Groundwater	Caliro et al. (2025b)
4.6	-	-	Groundwater	Caliro et al. (2025b)
3.7	-	-	Groundwater	Caliro et al. (2025b)
3.8	-	-	Groundwater	Caliro et al. (2025b)
3.9	-	-	Groundwater	Caliro et al. (2025b)
3.1	-	-	Groundwater	Caliro et al. (2025b)
4.6	-	-	Groundwater	Caliro et al. (2025b)
4.5	-	-	Groundwater	Caliro et al. (2025b)
4.1	-	-	Groundwater	Caliro et al. (2025b)
4.2	-	-	Groundwater	Caliro et al. (2025b)
4.4	-	-	Groundwater	Caliro et al. (2025b)
4.0	-	-	Groundwater	Caliro et al. (2025b)
3.0	-	-	Groundwater	Caliro et al. (2025b)
2.5	-	-	Groundwater	Caliro et al. (2025b)
3.2	-	-	Groundwater	Caliro et al. (2025b)
4.2	-	-	Groundwater	Caliro et al. (2025b)
2.7	-	-	Groundwater	Caliro et al. (2025b)
3.3	-	-	Groundwater	Caliro et al. (2025b)
4.3	-	-	Groundwater	Caliro et al. (2025b)
4.3	-	-	Groundwater	Caliro et al. (2025b)
4.2	-	-	Groundwater	Caliro et al. (2025b)
4.8	-	-	Groundwater	Caliro et al. (2025b)
5.2	-	-	Groundwater	Caliro et al. (2025b)
5.0	-	-	Groundwater	Caliro et al. (2025b)
4.6	-	-	Groundwater	Caliro et al. (2025b)
5.5	-	-	Groundwater	Caliro et al. (2025b)
4.3	-	-	Groundwater	Caliro et al. (2025b)
3.7	-	-	Groundwater	Caliro et al. (2025b)
4.7	-	-	Groundwater	Caliro et al. (2025b)
3.3	-	-	Groundwater	Caliro et al. (2025b)
3.9	-	-	Groundwater	Caliro et al. (2025b)
3.1	-	-	Groundwater	Caliro et al. (2025b)
4.2	-	-	Groundwater	Caliro et al. (2025b)
3.9	-	-	Groundwater	Caliro et al. (2025b)
3.6	-	-	Groundwater	Caliro et al. (2025b)
5.1	-	-	Groundwater	Caliro et al. (2025b)

4.0	-	-	Groundwater	Caliro et al. (2025b)
3.9	-	-	Groundwater	Caliro et al. (2025b)
4.2	-	-	Groundwater	Caliro et al. (2025b)
5.3	-	-	Groundwater	Caliro et al. (2025b)
4.9	-	-	Groundwater	Caliro et al. (2025b)
5.7	-	-	Groundwater	Caliro et al. (2025b)
5.2	-	-	Groundwater	Caliro et al. (2025b)
3.9	-	-	Groundwater	Caliro et al. (2025b)
5.9	-	-	Groundwater	Caliro et al. (2025b)
4.4	-	-	Groundwater	Caliro et al. (2025b)
4.3	-	-	Groundwater	Caliro et al. (2025b)
5.8	-	-	Groundwater	Caliro et al. (2025b)
3.1	-	-	Groundwater	Caliro et al. (2025b)
5.6	-	-	Groundwater	Caliro et al. (2025b)
3.7	-	-	Groundwater	Caliro et al. (2025b)
3.8	-	-	Groundwater	Caliro et al. (2025b)
2.5	-	-	Groundwater	Caliro et al. (2025b)
4.3	-	-	Groundwater	Caliro et al. (2025b)
4.1	-	-	Groundwater	Caliro et al. (2025b)
4.5	-	-	Groundwater	Caliro et al. (2025b)

Supplementary Table 2. pCO_2 and pH values obtained from a seawater vertical profile performed immediately above the Fumose vent (SdF). Reported errors for pCO_2 are 1σ uncertainties. The depth is given in meters below sea level (b.s.l). Exc carbon for each seawater point was calculated in reference to the atmospheric equilibrium pCO_2 value of 420 µm.

Station	East X	North Y	Bottom Depth [m]	Depth [m]	pCO2 Max (µatm)	pCO2 (error +/-)	Excess carbon (mol/kg)	Excess carbon (µmol/kg)
SF2	423065	4519508	10	2	514	2.6	4.9E-05	49.3
SF2	423065	4519508	10	6	1560	7.8	2.7E-04	272.9
SF2	423065	4519508	10	10	6822	34.1	5.3E-04	532.2
SF2	423065	4519508	10	9.3	8028	40.1	5.7E-04	571.8

Secca delle ess of	pH
	8.10
	6.90
	6.05
	5.90